Available online at www.sciencedirect.com
SCIENCE DIRECT®
ELSEVIER
International Journal of Solids and Structures 42 (2005) 4436–4467
INTERNATIONAL JOURNAL OF SOLIDS and STRUCTURES
www.elsevier.com/locate/ijsolstr

Modelling of progressive interface failure under combined normal compression and shear stress

Marcin Białas *, Zenon Mróz

Institute of Fundamental Technological Research, Świętokrzyska 21, 00-049 Warsaw, Poland

Received 25 June 2004
Available online 16 February 2005

Abstract

The present work is concerned with an analysis of progressive interface failure under normal compressive stress and varying shear stress using the cohesive crack model. The softening model is assumed and frictional linear stress at contact is accounted for. A monotonic loading in anti-plane shear of an elastic plate bonded to a rigid substrate is considered. An analytical solution is obtained by neglecting the effect of minor shear stress component in the plate. The elastic and plate interface compliances are included into the analysis. Three types of solutions are distinguished in the progressive delamination analysis, namely short, medium and long plate solutions. The analysis of quasi-static progressive delamination process clarifies the character of critical points and post-critical response of the plate. The analytical solution provides a reference benchmark for numerical algorithms of analysis of progressive interface delamination. The case of a rigid–softening interface was treated in a companion paper, where also cyclic loading was considered.

Keywords: Interface; Debonding; Cohesive zone; Instability points

1. Introduction

An analysis of growth of interlayer damage and of the resulting failure at the interface is one of more important problems in mechanics of composite materials, rocks and ceramics. A comprehensive survey of research in this area can be found, for instance, in the article by Hutchinson and Suo (1991), who discussed mixed mode crack propagation using the Griffith energy condition. In this paper, we shall apply the cohesive crack model assuming the existence of a damage (or plastic) zone ahead of the crack. The interface

* Corresponding author. Present address: Research Center Jülich, Institute for Materials and Processing in Energy Systems, IWV-2, D-52425 Jülich, Germany. Tel.: +49 246 161 5096; fax: +49 246 161 6464.
E-mail addresses: mbialas@ippt.gov.pl (M. Białas), zmroz@ippt.gov.pl (Z. Mróz).

0020-7683/$ - see front matter © 2005 Elsevier Ltd. All rights reserved.
doi:10.1016/j.ijsolstr.2005.01.006

layer in this zone is assumed to undergo an elastic–plastic deformation and damage inducing plastic softening. We shall consider the case of compressive normal traction acting at the interface with accompanying frictional slip developing along the crack portion. For cyclic loading, a set of progressive and reverse slip zones develops at the interface and frictional hysteretic effects occur accompanying cyclic dissipation and wear of surface asperities. The coupling between the propagation of damage zone and the frictional dissipation due to altering slip orientation may then occur.

The cohesive zone model has been used by numerous researchers in investigating crack growth, cf. for instance, Ortiz (1996), Hillerborg et al. (1976), Yang and Ravi-Chandar (1997). However, the effects of interface friction have not been fully investigated. The interaction of asperities at cracked interfaces and associated effects were studied in some papers, cf. Gross and Mendelsohn (1989), Bennison and Lawn (1989), Evans and Hutchinson (1989). The analysis of asperity interaction and of effects of micro-dilatancy in problems of fiber pullout was presented by Mróz and Stupkiewicz (1995). The cyclic loading of an interface was investigated by Shen and Mróz (2000), Mróz and Shen (1999) and Mróz and Białas (accepted for publication). In fact, the coupled phenomena occur at the interface such as wear and damage growth, frictional slip and localized temperature effects, asperities crushing or flattening with the associated dilatancy phenomena.

The present work is aimed at formulation of progressive damage and slip at the contact interface under compressive normal stress and in-plane loading on the plate boundary. The analytical solution is referred to the case of anti-plane shear induced by tangential tractions. A cohesive zone is assumed ahead of crack tip with a linear softening response for the bond layer. The analysis clarifies the character of instability points occurring due to interaction of damage zone with the boundary and presents a quasi-static solution for the progressive delamination process. The analytical analysis is next verified by the finite element analysis of the plate delamination. A solution for a rigid–softening interface subjected to monotonic and cyclic shear loading is presented in a companion paper by Mróz and Białas (accepted for publication).

2. Problem formulation

Consider a plate resting on a rigid foundation as schematically presented in Fig. 1. The plate is bonded to the foundation by a thin interface layer of thickness much smaller than the plate thickness. The upper plate surface is acted on by surface tractions $\boldsymbol{t}$ inducing compressive normal stresses at contact interface. The edge traction $\boldsymbol{T}$ may induce three modes of delamination or their combination, namely opening, longitudinal and transverse shear modes, analogous to fundamental modes in fracture mechanics. Assuming the plate thickness to be small as compared to its other dimensions, its response may be described within linear elasticity equations and the interaction tractions of the bonding interface can be treated as in-plane body forces acting on the plate. If there is no opening mode at the interface, the plate deformation state can be described by assuming plane stress conditions.

By assuming that there is a frictional contact at the interface between the plate and the substrate governed by the Coulomb's law, the traction $\boldsymbol{t}$ normal to the upper plate surface induces the frictional stress

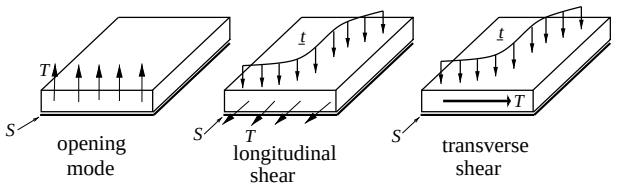

Fig. 1. Basic modes of delamination.

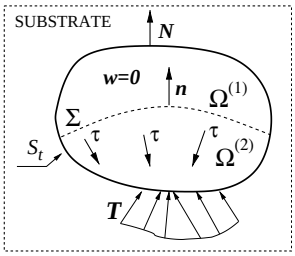

Fig. 2. A plate in plane stress condition resting on a rigid substrate.

having the magnitude $|\boldsymbol{\tau}| = \mu|\boldsymbol{t}|$. The friction stress direction remains unknown. When a rigid–frictional interface is assumed, we have two zones developed at the interface, namely $\Omega^{(1)}$, where the structure is fully bonded and $\Omega^{(2)}$, where the bond is damaged and there is a frictional contact. Let Σ denote the delamination front between regions $\Omega^{(1)}$ and $\Omega^{(2)}$, as schematically presented in Fig. 2. The displacement field $\boldsymbol{w}$ has to be continuous across Σ:

$$\lceil \boldsymbol{w} \rfloor = \boldsymbol{0}, \tag{1}$$

where $\lceil m(\boldsymbol{x}) \rfloor = m(\boldsymbol{x}^+) - m(\boldsymbol{x}^-)$, $\boldsymbol{x} \in \Sigma$ is the discontinuity of function $m(\boldsymbol{x})$ across Σ ($\boldsymbol{x}^+ = \boldsymbol{x}^-$, $\boldsymbol{x}^+ \in \Omega^{(1)}$, $\boldsymbol{x}^- \in \Omega^{(2)}$). On the other hand, for a rigid–frictional interface there is discontinuous switch of shear stresses at the interface across the boundary Σ:

$$\lceil \boldsymbol{\tau n} \rfloor \neq \boldsymbol{0}, \tag{2}$$

where $\boldsymbol{n}$ is a unit vector pointing into $\Omega^{(1)}$ and normal to the delamination front.

The time derivative of condition (1) provides a relation between the velocity field $\boldsymbol{v} = \dot{\boldsymbol{w}} = \partial \boldsymbol{w}/\partial t$ and the discontinuity of displacement gradient across Σ:

$$\lceil \dot{\boldsymbol{w}} \rfloor + v_{\mathrm{n}} \lceil (\nabla \boldsymbol{w}) \cdot \boldsymbol{n} \rfloor = \boldsymbol{0}, \tag{3}$$

where v_{n} is the velocity of delamination front. The frictional tractions at the interface can be treated as in-plane body forces, so the equation of equilibrium takes the form:

$$\mathrm{Div}\, \tilde{\boldsymbol{\sigma}} + \boldsymbol{\tau} = \boldsymbol{0}, \tag{4}$$

with $\tilde{\sigma}_{ij} = t\sigma_{ij}$ $(i,j = 1,2)$ being a stress tensor in the plane stress case. The interfacial frictional tractions satisfy the Coulomb's law:

$$\begin{aligned} &|\boldsymbol{\tau}| \leqslant \mu|\boldsymbol{t}| && \text{for } |\dot{\boldsymbol{w}}| = 0, \\ &|\boldsymbol{\tau}| = \mu|\boldsymbol{t}|, \ \ \boldsymbol{\tau}/|\boldsymbol{\tau}| = \dot{\boldsymbol{w}}/|\dot{\boldsymbol{w}}| && \text{for } |\dot{\boldsymbol{w}}| > 0. \end{aligned} \tag{5}$$

The boundary conditions on S_{t} are

$$\tilde{\boldsymbol{\sigma}} \boldsymbol{N} = \boldsymbol{T}, \tag{6}$$

where $\boldsymbol{N}$ is the unit normal vector to S_{t}. Additional boundary conditions on the delamination front Σ are provided by Eqs. (1) and (3) and have the form:

$$\lceil \boldsymbol{w} \rfloor = \boldsymbol{0}, \qquad \lceil \dot{\boldsymbol{w}} \rfloor = -v_{\mathrm{n}} \lceil (\nabla \boldsymbol{w}) \cdot \boldsymbol{n} \rfloor. \tag{7}$$

To fully formulate the delamination process for an elastic plate bonded to a rigid substrate, we define the strain rate tensor $\dot{\boldsymbol{\varepsilon}}$:

$$\dot{\boldsymbol{\varepsilon}} = \tfrac{1}{2}(\nabla \dot{\boldsymbol{w}} + \nabla^{\mathrm{T}} \dot{\boldsymbol{w}}) \tag{8}$$

and the linear constitutive equation for the plate material:

$$\dot{\tilde{\boldsymbol{\sigma}}} = \boldsymbol{C}\dot{\boldsymbol{\varepsilon}}, \tag{9}$$

where $\boldsymbol{C}$ is the elastic tensor.

The rate of dissipated energy is a difference between the rate of work done on the system by external forces $\boldsymbol{T}$ and the rate of change of elastic energy:

$$\dot{D} = \int_{S_t} \boldsymbol{T}\cdot\dot{\boldsymbol{w}}\,\mathrm{d}S - \frac{\mathrm{d}}{\mathrm{d}t}\int_{\Omega^{(2)}} U(\boldsymbol{\varepsilon})\,\mathrm{d}\Omega, \tag{10}$$

where $U(\boldsymbol{\varepsilon}) = \frac{1}{2}\boldsymbol{\varepsilon}\boldsymbol{C}\boldsymbol{\varepsilon}$ is the specific elastic energy per unit volume. The time derivative of the total elastic energy can be rewritten in the form:

$$\frac{\mathrm{d}}{\mathrm{d}t}\int_{\Omega^{(2)}} U(\boldsymbol{\varepsilon})\,\mathrm{d}\Omega = \int_{\Omega^{(2)}} \tilde{\boldsymbol{\sigma}}\cdot\dot{\boldsymbol{\varepsilon}}\,\mathrm{d}\Omega + \int_{\Sigma} U(\boldsymbol{\varepsilon})v_{\mathrm{n}}\,\mathrm{d}\Sigma, \tag{11}$$

where the fact, that the delamination front Σ changes with time and propagates during the loading process has been used to derive the second term on the right side of above equation. By substituting (4), (6), (7) and (11) into Eq. (10) and making use of Gauss theorem, we can write the formula for the rate of dissipated energy

$$D = \int_{\Omega^{(2)}} \boldsymbol{\tau}\cdot\dot{\boldsymbol{u}}\,\mathrm{d}\Omega + \int_{\Sigma}[(\tilde{\boldsymbol{\sigma}}\boldsymbol{n})\cdot(\nabla\boldsymbol{u}\cdot\boldsymbol{n}) - U(\boldsymbol{\varepsilon})]v_{\mathrm{n}}\,\mathrm{d}\Sigma. \tag{12}$$

The first term in the above equation refers to frictional dissipation at the interface, the second is related to the energy dissipated at the delamination front.

In the present paper, the bonding layer will be treated as an elastic–plastic softening interface for which the response is expressed in terms of contact stress components and the conjugate displacement discontinuities. As the substrate is assumed as rigid, the plate displacement field at the interface represents the displacement discontinuity for the interface. The constitutive equations for the interface will be referred to elastic, elastic–plastic and frictional slip regimes. We shall now discuss these relations in more detail.

2.1. Constitutive relations for the interface

Considering an interface S, we neglect the in-plane stress components and express the deformation response in terms of the interface traction components σ_{n}, τ_{l}, τ_{m}, where

$$\sigma = \boldsymbol{i}_{\mathrm{n}}\cdot\boldsymbol{\sigma}\boldsymbol{i}_{\mathrm{n}}, \qquad \tau_{\mathrm{l}} = \boldsymbol{i}_{\mathrm{l}}\cdot\boldsymbol{\sigma}\boldsymbol{i}_{\mathrm{n}}, \qquad \tau_{\mathrm{m}} = \boldsymbol{i}_{\mathrm{m}}\cdot\boldsymbol{\sigma}\boldsymbol{i}_{\mathrm{n}}, \tag{13}$$

and $\boldsymbol{i}_{\mathrm{n}}$ is the unit normal vector to S, $\boldsymbol{i}_{\mathrm{l}}$ and $\boldsymbol{i}_{\mathrm{m}}$ are the unit vectors within the S, forming the orthonormal basis. The displacement discontinuity vector $\boldsymbol{\delta}$ on S can also be decomposed into normal and tangential components δ_{n}, δ_{l} and δ_{m}. The total displacement discontinuity and its rate are decomposed into elastic and slip components, thus:

$$\boldsymbol{\delta} = \boldsymbol{\delta}^{\mathrm{e}} + \boldsymbol{\delta}^{\mathrm{s}}, \qquad \dot{\boldsymbol{\delta}} = \dot{\boldsymbol{\delta}}^{\mathrm{e}} + \dot{\boldsymbol{\delta}}^{\mathrm{s}}. \tag{14}$$

The constitutive equations relating the interface tractions and the reversible part of displacement discontinuity are of the form:

$$\dot{\sigma} = K_{\mathrm{n}}\dot{\delta}^{\mathrm{e}}_{\mathrm{n}}, \qquad \dot{\tau}_{\mathrm{l}} = K_{\mathrm{t}}\dot{\delta}^{\mathrm{e}}_{\mathrm{l}}, \qquad \dot{\tau}_{\mathrm{m}} = K_{\mathrm{t}}\dot{\delta}^{\mathrm{e}}_{\mathrm{m}}, \tag{15}$$

where K_{n} and K_{t} is an interfacial stiffness respectively in tension and shear. The irreversible part of displacement discontinuity is related to the failure process at the interface and expressed in the framework of theory of plasticity by an evolution of failure function F. The proposed failure function has the form:

$$F(\sigma,\tau)=\begin{cases}\tau+\mu\sigma-\tau_c(\delta_e)\leqslant 0 & \text{for } \sigma<0,\\ \sqrt{\left(\frac{\tau_c^0}{\sigma_c^0}\right)^2\sigma^2+\tau^2}-\tau_c(\delta_e)\leqslant 0 & \text{for } \sigma\geqslant 0,\end{cases}\tag{16}$$

where

$$\tau=\sqrt{\tau_l^2+\tau_m^2},$$

μ is a friction coefficient and $\tau_c(\delta_e)$ the critical shear stress for $\sigma=0$. The failure parameter δ_e is defined as

$$\delta_e=\int_0^t\sqrt{(\dot\delta_t^s)^2+M^2(\dot\delta_n^s)^2}\,d\bar t,\qquad \dot\delta_t^s=\sqrt{(\dot\delta_l^s)^2+(\dot\delta_m^s)^2},\tag{17}$$

where M is a material constant expressing the influence of opening mode on failure evolution.

Thus, for the compressive traction acting at the interface we have the Coulomb friction law relating the shear and normal stresses, whereas for tension the damage surface is an ellipse. The function F is presented in Fig. 3.

The assumed slip potential is of the form:

$$G(\sigma,\tau)=\begin{cases}\tau-\tau_c(\delta_e) & \text{for } \sigma<0,\\ \sqrt{\left(\frac{\tau_c^0}{\sigma_c^0}\right)^2\sigma^2+\tau^2}-\tau_c(\delta_e) & \text{for } \sigma\geqslant 0.\end{cases}\tag{18}$$

Thus, we have an associated flow rule for positive normal stresses and non-associated flow rule for interface subjected to compression. The reason for doing that is to neglect the contact dilatancy. It should be noted, that the slip rule remains continuous when the normal stress σ changes sign, though the damage function F has a slope discontinuity for $\sigma=0$, see Fig. 3.

The sliding rule has a form:

$$\dot\delta_t^s=\dot\lambda\frac{\partial G}{\partial\tau},\qquad \dot\delta_n^s=\dot\lambda\frac{\partial G}{\partial\sigma},\qquad F\leqslant 0,\qquad \dot\lambda F=0,\tag{19}$$

where $\dot\lambda$ is a positive slip multiplier.

The evolution equation expresses the failure development at the interface and relates the increasing separation $\boldsymbol{\delta}^s$ with the vanishing interfacial traction. In the present study, the linearly decreasing function has been assumed:

$$\tau_c(\delta_e)=\begin{cases}\tau_c^0-K_r\delta_e & \delta_e<\frac{\tau_c^0}{K_r},\\ 0 & \delta_e\geqslant\frac{\tau_c^0}{K_r},\end{cases}\tag{20}$$

allowing for an analytical solution of anti-plane shear state presented in the following section.

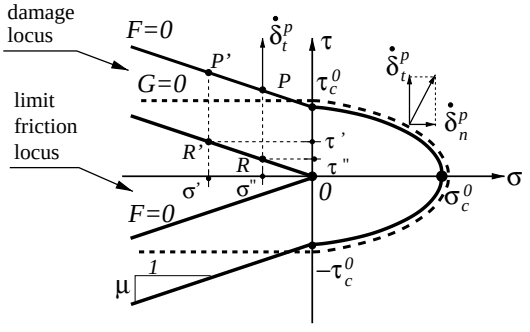

Fig. 3. Yield function F and plastic potential G.

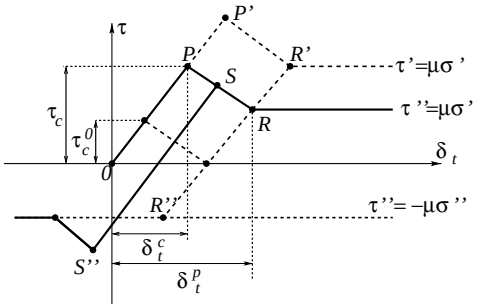

Fig. 4. Stress–displacement response for elastic–plastic layer under constant compressive normal stress.

In the case of monotonically varying shear loading and constant compressive normal traction $\sigma = \text{constant}$, Eq. (19) can be integrated in order to provide the total slip displacement:

$$\delta_{\mathrm{t}}^{\mathrm{s}} = \lambda \frac{\partial G}{\partial \tau} = \lambda, \qquad F^{\mathrm{f}} \leqslant 0, \qquad \lambda F^{\mathrm{f}} = 0. \tag{21}$$

However, when unloading and reverse slip occurs, the memory of the previous slip displacement must be stored and added to the reverse slip displacement. Fig. 4 presents the shear stress–tangential sliding response for the interface layer in the case of progressive delamination. For specified σ, the shear stress first reaches the maximum critical value τ_{c} and then in the elasto-plastic softening process, decreases to the limit friction value $\mu\sigma$ in the fully damaged state. We can therefore write:

$$\tau = K_{\mathrm{t}}\delta_{\mathrm{t}}, \quad 0 < \delta_{\mathrm{t}} < \delta_{\mathrm{t}}^{c} = \frac{\tau_{\mathrm{c}}}{K_{\mathrm{t}}}, \tag{22}$$

$$\tau = \tau_{\mathrm{c}} - K_{\mathrm{s}}(\delta_{\mathrm{t}} - \delta_{\mathrm{t}}^{c}), \quad \delta_{\mathrm{t}}^{c} < \delta_{\mathrm{t}} < \delta_{\mathrm{t}}^{\mathrm{p}} = \delta_{\mathrm{t}}^{c} + \frac{\tau_{\mathrm{c}} - \mu\sigma}{K_{\mathrm{s}}}, \tag{23}$$

$$\tau = \mu\sigma, \quad \delta_{\mathrm{t}} > \delta_{\mathrm{t}}^{\mathrm{p}}, \tag{24}$$

where $K_{\mathrm{s}} > 0$ is the elasto-plastic softening modulus.

Assuming the decomposition (14), we can write in the softening regime:

$$\dot{\delta}_{\mathrm{t}} = \dot{\delta}_{\mathrm{t}}^{\mathrm{e}} + \dot{\delta}_{\mathrm{t}}^{\mathrm{s}} = \frac{\dot{\tau}}{K_{\mathrm{t}}} - \frac{\dot{\tau}}{K_{\mathrm{r}}} = -\frac{\dot{\tau}}{K_{\mathrm{s}}}, \tag{25}$$

where K_{r} is the softening modulus associated with the plastic slip component $\delta_{\mathrm{t}}^{\mathrm{s}}$. From Eq. (25) we have

$$\frac{1}{K_{\mathrm{s}}} = \frac{1}{K_{\mathrm{r}}} - \frac{1}{K_{\mathrm{t}}}, \qquad K_{\mathrm{s}} = \frac{K_{\mathrm{r}}}{1 - K_{\mathrm{r}}/K_{\mathrm{t}}}. \tag{26}$$

Thus, the softening response for the elasto-plastic interface is dependent on the ratio $K_{\mathrm{r}}/K_{\mathrm{t}}$. When $\zeta = K_{\mathrm{r}}/K_{\mathrm{t}} = 1$, we have the brittle response of the interface. On the other hand, when $K_{\mathrm{t}} \to \infty$, that is for rigid–plastic response, there is $K_{\mathrm{s}} = K_{\mathrm{r}}$.

The discussion of a dilatant contact condition can be found in the paper by Mróz and Seweryn (1998).

2.2. Anti-plane shear state

In the present section we shall formulate equations of an anti-plane shear state allowing for analytical solution of delamination process. Let us consider a plate of length L, width b, and thickness t, bonded to a rigid foundation by an interface layer of thickness h, $h \ll t$, as shown in Fig. 5.

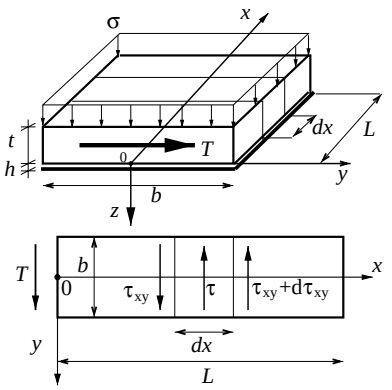

Fig. 5. Plate bonded to the substrate. Anti-plane shear state $b > L$.

The uniform compressive traction $\sigma_{zz} = -\sigma$ is assumed to act at the upper plate surface. The plate is loaded by the shear force $T = \tau_{yx}(0)A$, $A = bt$, at the end section $x = 0$. The other end at $x = L$ remains traction free. Assuming the transverse dimension b to be larger than the plate length L, the flexural effects can be neglected and the state of anti-plane shear can be assumed with two shear stress components τ_{yx} and τ_{yz}, so that the equilibrium equation is:

$$\frac{\partial \tau_{yx}}{\partial x} + \frac{\partial \tau_{yz}}{\partial z} = 0, \tag{27}$$

and $\sigma_{zz} = -\sigma = \text{constant}$ is the initial stress induced by the lateral compressive traction along the z-axis. Denoting by $w = w(x, z)$ the displacement field along the y-axis and using the Hooke's law:

$$\tau_{yz} = -G_2 \frac{\partial w}{\partial z}, \qquad \tau_{xy} = -G_1 \frac{\partial w}{\partial x}, \tag{28}$$

the equilibrium equation (27) takes the form:

$$G_1 \frac{\partial^2 w}{\partial x^2} + G_2 \frac{\partial^2 w}{\partial z^2} = 0, \tag{29}$$

where G_1 and G_2 are the shear moduli along x and z axes. The boundary conditions at the interface $z = 0$: $\tau_{yz} = -\tau_f$; at the upper boundary $z = -t$: $\tau_{yz} = 0$ and at the transverse boundaries $x = 0$: $\tau_{xy}(0) = f_0(y, z)$, $x = L$: $\tau_{xy}(L) = 0$ should be satisfied.

A simplified solution can be generated by assuming the distribution of τ_{yz}, namely:

$$\tau_{yz} = -\tau(x)\left(1 + \frac{z}{t}\right), \tag{30}$$

where $\tau(x)$ is the interface shear stress at $z = 0$. The equilibrium (27) takes the form:

$$\frac{\partial \tau_{xy}}{\partial x} + \frac{\tau}{t} = 0. \tag{31}$$

Let us note that this form of (31) can be obtained by assuming the *shear beam model*, that is assuming $w = w(x)$, $\tau_{xy} = -G\mathrm{d}w/\mathrm{d}x$ and writing the equilibrium equation for the elastic beam interacting with the interface cohesive layer:

$$A \frac{\mathrm{d}\tau_{xy}}{\mathrm{d}x} + b\tau = 0, \tag{32}$$

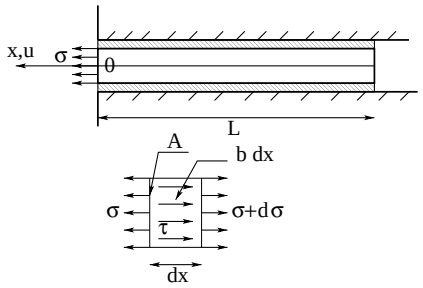

Fig. 6. Fiber pullout.

where $A = bt$ denotes the transverse cross section area. This formula can be rewritten in the form:

$$-AG\frac{\mathrm{d}^2 w}{\mathrm{d}x^2} + b\tau = 0. \tag{33}$$

This form of equation can be generated from (29) by assuming $G_2 \to \infty$, that is neglecting shear deformation along the z-axis and regarding the shear stress τ_{yz} as a reaction. Alternatively, this equation can be obtained from (29) and (30) by satisfying the equilibrium equation at the interface $z = 0$. In the following, we shall provide the analytical solution using the simplified equation.

It should be noted, that the same set of equations apply for a fiber pullout problem as presented in Fig. 6. By assuming the problem to be axisymmetric and reflecting the deformable medium surrounding the fiber by the interface constitutive equation with the surrounding medium to be rigid, one obtains the equilibrium equation

$$A\frac{\mathrm{d}\sigma}{\mathrm{d}x} + b\tau = 0. \tag{34}$$

The three dimensional effects associated with normal stresses due to Poisson's ratio are then ignored. Additionally, treating the fiber as an elastic body, we have the linear constitutive relation between displacement field u and normal stress σ:

$$\sigma = -E\frac{\mathrm{d}u}{\mathrm{d}x}, \tag{35}$$

with E being the Young modulus. By substituting (34) into (35), one obtains a differential equation in the form:

$$-AE\frac{\mathrm{d}^2 u}{\mathrm{d}x^2} + b\tau = 0 \tag{36}$$

identical to (33). The results of fiber pullout based on such a one dimensional model of decohesion were discussed by Schreyer and Peffer (2000).

3. Analytical solution

In the following we shall assume progressive damage at the material interface and examine the effect of progressive delamination on stress and displacement fields.

By substituting Eqs. (22)–(24) into (33), one obtains ordinary differential equations providing formulas for displacement fields w^{e}, w^{p} and w^{f}, respectively for elastic, plastic and frictional interfaces. Thus, for the elastic case we have:

$$w^{\mathrm{e}}(x) = C_1 e^{rx} + C_2 e^{-rx}, \quad r = \sqrt{\frac{K_{\mathrm{t}}}{Gt}}, \tag{37}$$

whereas the displacement field within the plastic zone is given by the following formula:

$$w^{\mathrm{p}}(x) = C_3 \cos(r_{\mathrm{s}} x) + C_4 \sin(r_{\mathrm{s}} x) + \frac{\tau_{\mathrm{c}}}{K_{\mathrm{s}}} + \frac{\tau_{\mathrm{c}}}{K_{\mathrm{t}}}, \quad r_{\mathrm{s}} = \sqrt{\frac{K_{\mathrm{s}}}{Gt}}. \tag{38}$$

In the case of frictional interface, the displacement field takes the form:

$$w^{\mathrm{f}}(x) = \operatorname{sign}(\dot{w}) \frac{\mu\sigma}{2Gt} x^2 + C_5 x + C_6. \tag{39}$$

In the above formulas C_1, C_2, C_3, C_4, C_5 and C_6 are the integration constants to be specified from boundary and continuity conditions.

We shall assume monotonic damage at the material interface and examine the effect of progressive delamination on stress and displacement fields. In order to do that, we shall combine functions (37)–(39) using appropriate boundary and continuity conditions. Three different solution types can be distinguished, each being defined by the plate dimensions. They are characterized in the following sections where the consecutive stages of delamination process are described.

3.1. Short plate solution

The interface is elastic during the first stage of loading. The plate displacement field is provided by Eq. (37) with the integration constants C_1 and C_2 to be specified from the boundary conditions:

$$w^{\mathrm{e}\prime}(L) = 0, \qquad w^{\mathrm{e}}(0) = w_0, \tag{40}$$

with w_0 being the displacement of loaded end $x = 0$ and $w^{\mathrm{e}\prime}$ denoting the slope of the deflection curve. The displacement field w^{e} takes the form:

$$w^{\mathrm{e}}(x, w_0) = w_0 \frac{\cosh[r(L-x)]}{\cosh(Lr)}. \tag{41}$$

The corresponding τ_{xy} stress can be obtained from Eq. (28):

$$\tau^{\mathrm{e}}_{xy}(x, w_0) = w_0 Gr \frac{\sinh[r(L-x)]}{\cosh(Lr)}. \tag{42}$$

Formula (33) provides the shear stress at the plastic interface:

$$\tau^{\mathrm{e}}(x, w_0) = K_{\mathrm{t}} w_0 \frac{\cosh[r(L-x)]}{\cosh(rL)}. \tag{43}$$

When the displacement w_0 reaches the value $\tau_{\mathrm{c}}/K_{\mathrm{t}}$, the plastic zone appears at the loaded end, as presented schematically in Fig. 7 and the second delamination phase begins. The elastic zone displacement field can be obtained from Eq. (37) with the integration constants satisfying the conditions:

$$w^{\mathrm{e}\prime}(L) = 0, \qquad w^{\mathrm{e}}(s_1) = \frac{\tau_{\mathrm{c}}}{K_{\mathrm{t}}}.$$

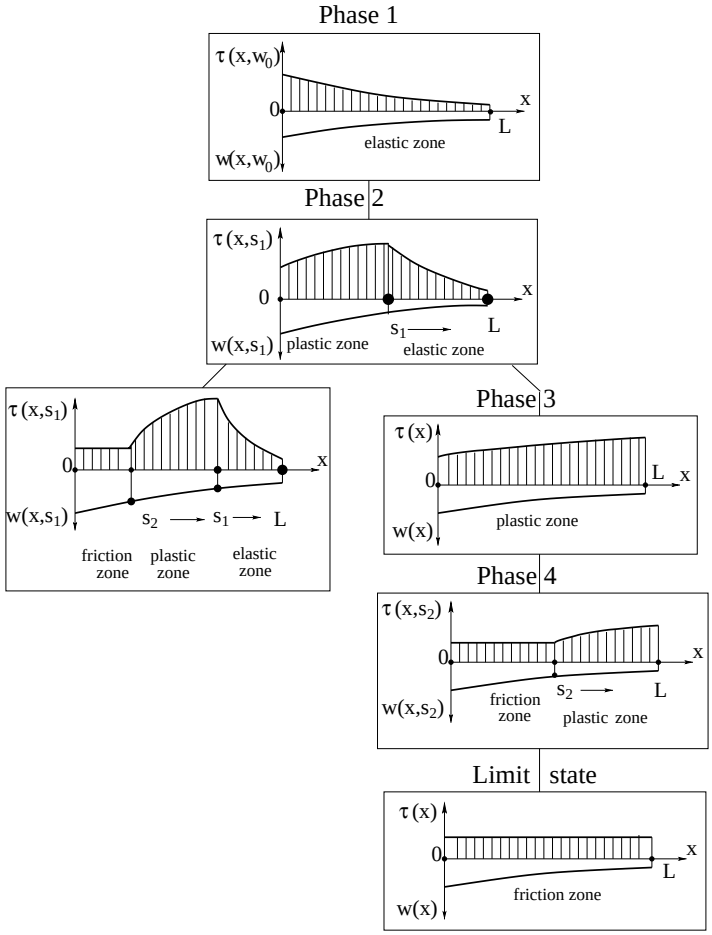

Fig. 7. Short plate solution. Delamination phases.

The value of s_1 specifies the coordinate of the transition point between elastic and plastic (cohesive) zones. The stress and displacement fields within the elastic zone take the form:

$$w^{\mathrm{e}}(x,s_1)=\frac{\tau_{\mathrm{c}}}{K_{\mathrm{t}}}e^{-rL}\frac{e^{r(2L+s_1)}+e^{r(2x+s_1)}}{e^{2Lr}+e^{2rs_1}}, \tag{44}$$

$$\tau^{\mathrm{e}}_{xy}(x,s_1)=2Gr\frac{\tau_{\mathrm{c}}}{K_{\mathrm{t}}}\frac{e^{r(L+s_1)}}{e^{2Lr}+e^{2rs_1}}\sinh[r(L-x)], \tag{45}$$

$$\tau^{\mathrm{e}}(x,s_1)=2K_{\mathrm{s}}\frac{\tau_{\mathrm{c}}}{K_{\mathrm{t}}}\frac{e^{r(L+s_1)}}{e^{2Lr}+e^{2rs_1}}\cosh[r(L-x)]. \tag{46}$$

The displacement field within the plastic zone is provided by Eq. (38) with the integration constants C_3 and C_4 specified from the continuity conditions:

$$w^{\mathrm{p}}(s_1)=w^{\mathrm{e}}(s_1)=\frac{\tau_{\mathrm{c}}}{K_{\mathrm{t}}},\qquad w^{\mathrm{p}\prime}(s_1)=w^{\mathrm{e}\prime}(s_1).$$

The resultant stress and displacement fields take the form:

$$w^{\mathrm{p}}(x,s_1)=\frac{\tau_{\mathrm{c}}}{K_{\mathrm{t}}}\left\{1-\frac{r}{r_{\mathrm{s}}}H\sin[r_{\mathrm{s}}(s_1-x)]\right\}+\frac{\tau_{\mathrm{c}}}{K_{\mathrm{s}}}\{1-\cos[r_{\mathrm{s}}(x-s_1)]\}, \tag{47}$$

$$\tau^{\mathrm{p}}_{xy}(x,s_1)=-Gr_{\mathrm{s}}\frac{\tau_{\mathrm{c}}}{K_{\mathrm{s}}}\sin[r_{\mathrm{s}}(x-s_1)]-Gr\frac{\tau_{\mathrm{c}}}{K_{\mathrm{t}}}H\cos[r_{\mathrm{s}}(s_1-x)], \tag{48}$$

$$\tau^{\mathrm{p}}(x,s_1)=\tau_{\mathrm{c}}\cos[r_{\mathrm{s}}(x-s_1)]+\tau_{\mathrm{c}}\frac{r_{\mathrm{s}}}{r}H\sin[r_{\mathrm{s}}(s_1-x)], \tag{49}$$

with $H=\tanh[r(s_1-L)]$.

The short plate solution takes place when the plate is short enough for the plastic zone to cover the entire length L. This is true when the following condition is satisfied:

$$w^{\mathrm{p}}(x=0,s_1=L)\leqslant w_{\mathrm{p}}=\frac{\tau_{\mathrm{c}}}{K_{\mathrm{t}}}+\frac{\tau_{\mathrm{c}}-\mu\sigma}{K_{\mathrm{s}}}, \tag{50}$$

stating that there is no frictional zone developed at the interface while its elastic part has finally vanished. The inequality (50) reduces to

$$\frac{L}{t}\leqslant\sqrt{\frac{G}{K_{\mathrm{s}}t}}\arccos\frac{\mu\sigma}{\tau_{\mathrm{c}}}, \tag{51}$$

where the condition put on the plate dimensions is shown explicitly. This condition may be rewritten in a dimensionless form:

$$\chi\leqslant\arccos\eta,\qquad\chi=r_{\mathrm{s}}L,\qquad\eta=\frac{\mu\sigma}{\tau_{\mathrm{c}}}, \tag{52}$$

requiring the dimensionless parameter χ to be bounded. In a particular case, we can vary the softening modulus K_{s} keeping the plate length constant and, as a result, we will obtain a short plate solution. It is seen that the system response depends on a complex interaction between mechanical and geometrical characteristics to be captured by two dimensionless parameters χ and η.

There is only plastic zone at the interface during the third loading phase, as presented schematically in Fig. 7. The displacement field is given by Eq. (38), where the integration constants can be specified from the boundary conditions:

$$w^{\mathrm{p}\prime}(L)=0,\qquad w^{\mathrm{p}}(0)=w^{\mathrm{p}}_0, \tag{53}$$

with w^{p}_0 being the loaded end displacement. At this stage, the value of w^{p}_0 becomes the control parameter. The displacement field, shear stress τ^{p}_{xy} and interfacial traction τ^{p} fields are:

$$w^{\mathrm{p}}(x,w^{\mathrm{p}}_0)=\left(w^{\mathrm{p}}_0-\frac{\tau_{\mathrm{c}}}{K_{\mathrm{s}}}-\frac{\tau_{\mathrm{c}}}{K_{\mathrm{t}}}\right)\frac{\cos[r_{\mathrm{s}}(L-x)]}{\cos(r_{\mathrm{s}}L)}+\frac{\tau_{\mathrm{c}}}{K_{\mathrm{s}}}+\frac{\tau_{\mathrm{c}}}{K_{\mathrm{t}}},\quad 0\leqslant x\leqslant L, \tag{54}$$

$$\tau^{\mathrm{p}}_{xy}(x,w^{\mathrm{p}}_0)=-Gr_{\mathrm{s}}\left(w^{\mathrm{p}}_0-\frac{\tau_{\mathrm{c}}}{K_{\mathrm{s}}}-\frac{\tau_{\mathrm{c}}}{K_{\mathrm{t}}}\right)\frac{\sin[r_{\mathrm{s}}(L-x)]}{\cos(r_{\mathrm{s}}L)},\quad 0\leqslant x\leqslant L, \tag{55}$$

$$\tau^{\mathrm{p}}(x,w^{\mathrm{p}}_0)=\left(\frac{\tau_{\mathrm{c}}}{K_{\mathrm{t}}}+\frac{\tau_{\mathrm{c}}}{K_{\mathrm{s}}}-w^{\mathrm{p}}_0\right)\frac{\cos[r_{\mathrm{s}}(L-x)]}{\sin(r_{\mathrm{s}}L)},\quad 0\leqslant x\leqslant L. \tag{56}$$

A friction zone starts to develop at the interface for the displacement w^{p}_0 reaching $w_{\mathrm{p}}=(\tau_{\mathrm{c}}-\mu\sigma)/K_{\mathrm{s}}+\tau_{\mathrm{c}}/K_{\mathrm{t}}$ and a subsequent loading phase begins, as presented in Fig. 7. There are two interfacial zones, namely

plastic and friction with respective displacement fields given by Eqs. (38) and (39). The integration constants are specified from the boundary and continuity conditions:

$$w^{p\prime}(L) = 0, \qquad w^{p}(s_2) = w^{f}(s_2) = \frac{\tau_c - \mu\sigma}{K_s} + \frac{\tau_c}{K_t}, \qquad w^{p\prime}(s_2) = w^{f\prime}(s_2), \tag{57}$$

where s_2 is a coordinate of the transition point between plastic and frictional zones. The displacement and stress fields take the form:

- plastic zone, $s_2 \leqslant x \leqslant L$:

$$w^{p}(x, s_2) = \frac{\tau_c}{K_t} + \frac{\tau_c}{K_s} - \frac{\mu\sigma}{K_s}\frac{\cos[r_s(L-x)]}{\cos[r_s(L-s_2)]}, \tag{58}$$

$$\tau^{p}_{xy}(x, s_2) = \frac{\mu\sigma}{K_s} r_s G \frac{\sin[r_s(L-x)]}{\cos[r_s(L-s_2)]}, \tag{59}$$

$$\tau^{p}(x, s_2) = \mu\sigma \frac{\cos[r_s(L-x)]}{\cos[r_s(L-s_2)]}; \tag{60}$$

- friction zone, $0 \leqslant x \leqslant s_2$:

$$w^{f}(x, s_2) = \frac{\mu\sigma}{2Gt}(x - s_2)^2 + \frac{\mu\sigma r_s}{K_s}\tan[r_s(L-s_2)](x-s_2) + \frac{\tau_c - \mu\sigma}{K_s} + \frac{\tau_c}{K_t}, \tag{61}$$

$$\tau^{f}_{xy}(x, s_2) = -\frac{\mu\sigma}{t}(x - s_2) - \frac{\mu\sigma r_s G}{K_s}\tan[r_s(L-s_2)], \tag{62}$$

$$\tau^{f}(x, s_2) = \mu\sigma, \tag{63}$$

so for this loading phase the value of s_2 takes over w^0_p as the control parameter and its monotonic increase describes the damage growth.

For s_2 equal to L the interface has been fully damaged and progressive delamination is accomplished. The limit shear stress subjected to the plate equals

$$\tau^{lim}_{xy}(0) = \frac{\mu\sigma}{t}L, \tag{64}$$

and is equilibrated by the frictional forces at the interface.

Fig. 8 presents relations between the loading traction $\tau_{xy}(0)$ and the loaded end displacement $w(0)$ for various values of dimensional parameters $\chi = r_s L$ and $\zeta = K_r/K_t$, where K_r is the softening modulus associated with the plastic slip component and K_t is the interface elasticity coefficient. Thus, the dimensionless parameter ζ describes the effect of interface compliance and its softening response. The condition (52), defining a short plate solution in terms of χ and η, is satisfied. Fig. 8(a) presents the influence of parameter χ that can be interpreted as the plate length L or the interface softening modulus K_s. Fig. 8(b) presents the effect of interfacial elasticity defined by the value of ζ. The dashed line is a solution obtained for an interface with no softening effect, simply frictional model. The sudden drop in the $\tau_{xy}(0)$ value is caused by the end effect, that is the interaction between the interfacial cohesive zone and the stress free end at $x = L$. It is seen, that the delamination process cannot be executed by stress controlled loading. Such a procedure would lead to a dynamic, unstable response. It is presented in Fig. 8(a) that the normalized maximum traction $\tau_{xy}(0)/\tau^{lim}_{xy}(0)$ subjected to the plate becomes higher as the length L, that is the dimensionless parameter χ, decreases. Thus, for a smaller plate we have a higher normalized strength of the structure. This scale effect is a result of softening law used for the material interface. The solution presented in Fig. 8(b) for $\zeta = 0$

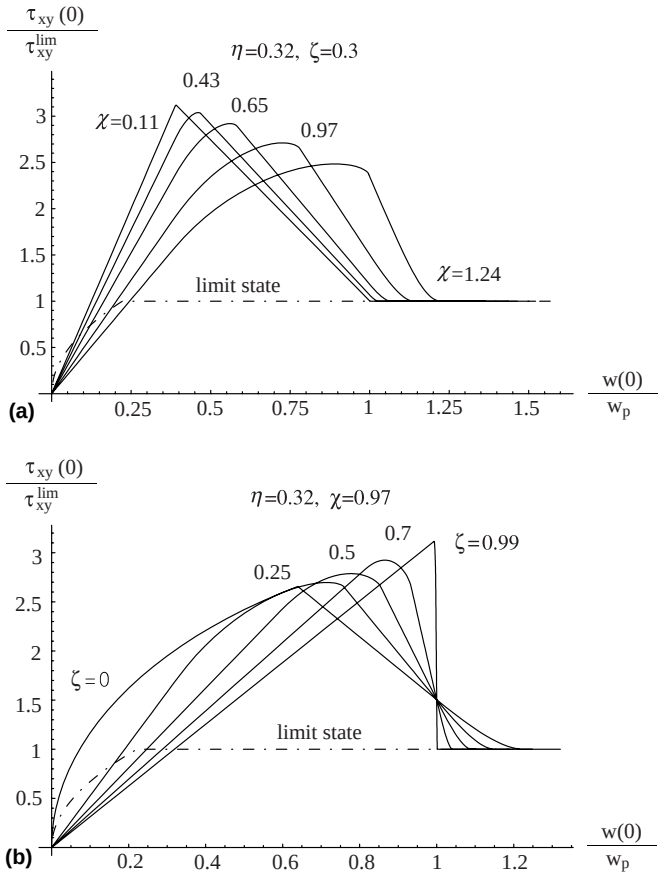

Fig. 8. Short plate solution. The loading traction $\tau_{xy}(0)$ versus loaded end displacement $w(0)$ for: (a) various values of $\chi = r_s L$—the influence of plate length L; (b) various values of $\zeta = K_t/K_t$—the influence of interface compliance with respect to its softening response; $\zeta = 0$, rigid–softening–frictional interface; $\zeta = 1$, perfectly brittle interface. The dashed line refers to the rigid–frictional model of the interface.

refers to rigid–plastic frictional interface. For subsequent values of ζ the interface becomes more compliant with respect to its softening behaviour. For the value of $\zeta = 1$ we have a brittle fracture of the bonding. It is seen that the interfacial elasticity can change the structure response significantly, though it does not enter the criterion (52) for a short plate solution.

3.2. Medium length solution

Let us assume now that the condition (51) is not satisfied and, as a result, there are following interface zones developed during the third loading phase: friction, plastic and elastic, as schematically presented in Fig. 9. The displacement fields for elastic, plastic and friction zones are given by Eqs. (37)–(39) respectively. The integration constants can be specified from the boundary and continuity conditions:

$$w^{e\prime}(L) = 0, \qquad w^{e}(s_1) = w^{p}(s_1) = \frac{\tau_c}{K_t}, \qquad w^{e\prime}(s_1) = w^{p\prime}(s_1), \tag{65}$$

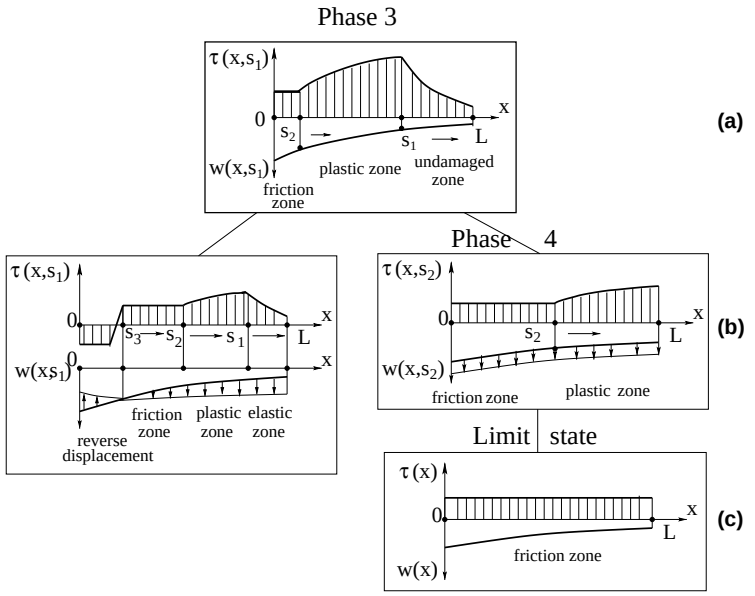

Fig. 9. Medium plate solution. Delamination phases.

$$w^{\mathrm{p}}(s_2) = w^{\mathrm{f}}(s_2) = \frac{\tau_{\mathrm{c}}}{K_{\mathrm{t}}} + \frac{\tau_{\mathrm{c}} - \mu\sigma}{K_{\mathrm{s}}}, \qquad w^{\mathrm{p}\prime}(s_2) = w^{\mathrm{f}\prime}(s_2), \tag{66}$$

where, as before, s_1 is the coordinate of the transition point between elastic and plastic regions, and s_2 indicates the point between plastic and undamaged zones. Assume that s_1 is now a monotonically increasing control parameter of the loading process and both shear stress and displacement at the loaded boundary $x = 0$ are specified in terms of s_1. With s_1 being the loading parameter, it subsequently follows from the conditions (65) and (66):

$$s_2 = s_1 - \frac{2}{r_{\mathrm{s}}} \arctan \frac{Hr_{\mathrm{s}}/r + \sqrt{1 + (Hr_{\mathrm{s}}/r)^2 - \eta^2}}{1 + \eta}, \tag{67}$$

with $H = \tanh[r(s_1 - L)]$. The displacement and stress fields are:

- elastic zone: $s_1 \leqslant x \leqslant L$,

$$w^{\mathrm{e}}(x, s_1) = \frac{\tau_{\mathrm{c}}}{K_{\mathrm{t}}} e^{-rL} \frac{e^{r(2L+s_1)} + e^{r(2x+s_1)}}{e^{2Lr} + e^{2rs_1}}, \tag{68}$$

$$\tau^{\mathrm{e}}_{xy}(x, s_1) = 2Gr \frac{\tau_{\mathrm{c}}}{K_{\mathrm{t}}} \frac{e^{r}(L + s_1)}{e^{2Lr} + e^{2rs_1}} \sinh[r(L - x)], \tag{69}$$

$$\tau^{\mathrm{e}}(x, s_1) = 2K_{\mathrm{s}} \frac{\tau_{\mathrm{c}}}{K_{\mathrm{t}}} \frac{e^{r}(L + s_1)}{e^{2Lr} + e^{2rs_1}} \cosh[r(L - x)]; \tag{70}$$

- plastic zone: $s_2 \leqslant x < s_1$,

$$w^{\mathrm{p}}(x, s_1) = \frac{\tau_{\mathrm{c}}}{K_{\mathrm{t}}} \left\{ 1 - \frac{r}{r_{\mathrm{s}}} H \sin[r_{\mathrm{s}}(s_1 - x)] \right\} + \frac{\tau_{\mathrm{c}}}{K_{\mathrm{s}}} \{1 - \cos[r_{\mathrm{s}}(x - s_1)]\}, \tag{71}$$

$$\tau^{\mathrm{p}}_{xy}(x,s_1) = -Gr_{\mathrm{s}}\frac{\tau_{\mathrm{c}}}{K_{\mathrm{s}}}\sin[r_{\mathrm{s}}(x-s_1)] - Gr\frac{\tau_{\mathrm{c}}}{K_{\mathrm{t}}}H\cos[r_{\mathrm{s}}(s_1-x)], \tag{72}$$

$$\tau^{\mathrm{p}}(x,s_1) = \tau_{\mathrm{c}}\cos[r_{\mathrm{s}}(x-s_1)] + \tau_{\mathrm{c}}\frac{r_{\mathrm{s}}}{r}H\sin[r_{\mathrm{s}}(s_1-x)]; \tag{73}$$

- friction zone: $0 \leqslant x < s_2$,

$$w^{\mathrm{f}}(x,s_1) = \frac{\mu\sigma}{2Gt}(x-s_2)^2 + \frac{r_{\mathrm{s}}}{K_{\mathrm{s}}}(x-s_2)Z + \frac{\tau_{\mathrm{c}}}{K_{\mathrm{t}}} + \frac{\tau_{\mathrm{c}}-\mu\sigma}{K_{\mathrm{s}}}, \tag{74}$$

$$\tau^{\mathrm{f}}_{xy}(x,s_1) = -\frac{\mu\sigma}{t}(x-s_2) - \frac{r_{\mathrm{s}}}{K_{\mathrm{s}}}GZ, \tag{75}$$

$$\tau^{\mathrm{f}}(x,s_1) = \mu\sigma; \tag{76}$$

where

$$Z = -\sqrt{1-\eta^2+\tanh^2[r(s_1-L)]K_{\mathrm{s}}/K_{\mathrm{t}}}. \tag{77}$$

Eq. (67) provides s_2 as a function of s_1.

One should remember that the formulas (74)–(76) are valid for monotonic interface loading only, that is when the following condition is satisfied:

$$\dot{w}^{\mathrm{f}} \geqslant 0. \tag{78}$$

With s_1 being the loading parameter during the third delamination stage, the inequality (78) can be rewritten as

$$\frac{\partial w^{\mathrm{f}}(x,s_1)}{\partial s_1} \geqslant 0 \tag{79}$$

stating, that the fully damaged interface slides forward. However, the above derivative changes sign indicating that there exists a zone where the interface is unloaded and the resultant interfacial stress are lower than $\tau = \mu\sigma$. In other words, the plate exhibits reverse displacements, as schematically presented in Fig. 9. Let s_3 be the value of x where the derivative $\partial w^{\mathrm{f}}(x,s_1)/\partial s_1$ vanishes:

$$\frac{\partial w^{\mathrm{f}}(x,s_1)}{\partial s_1} = 0, \tag{80}$$

and becomes negative for $0 \leqslant x \leqslant s_3$. The condition (80) determines the position of a transition point between the forward ($\dot{w} > 0$) and the reverse displacement zone ($\dot{w} < 0$). By substituting (74) into Eq. (80), one obtains:

$$s_3 = s_2 - 2\cosh d \times \frac{r(r^2-3r_{\mathrm{s}}^2)\eta Z\cosh d - (r^2+r_{\mathrm{s}}^2)(r\eta Z\cosh 3d - 4r_{\mathrm{s}}\sinh d)}{r_{\mathrm{s}}r\{r_{\mathrm{s}}^2(3\eta^2-8) - (r\eta)^2 + \eta[4r_{\mathrm{s}}^2\cosh 2d + (r^2+r_{\mathrm{s}}^2)\cosh 4d]\}}, \tag{81}$$

where

$$d = r(L-s_1),$$

and Z is given by Eq. (77). Formula (81) is an increasing function of s_1 meaning that the length of reverse slip zone increases while the elastic zone becomes shorter, that is the control parameter s_1 approaches L. The value of $s_3(s_1 = L)$ is the length of reverse slip zone at the instant when the elastic interfacial area vanishes. It becomes obvious that the inequality

$$s_3(s_1 = L) \leqslant 0$$

provides a condition for no reverse displacement zone at the interface during third loading phase. The above inequality is satisfied for the length to height ratio L/t smaller than

$$\frac{L}{t} < \sqrt{\frac{G}{K_s t}}\left(\arccos\eta + \frac{\eta}{\sqrt{1-\eta^2}}\right), \tag{82}$$

or (in a dimensionless form):

$$\chi \leqslant \arccos\eta + \frac{\eta}{\sqrt{1-\eta^2}}, \quad \chi = r_s L, \ \ \eta = \frac{\mu\sigma}{\tau_c}. \tag{83}$$

A plate satisfying the inequality (83) will provide a medium length solution. In a dimensionless form, it is defined by the following formula:

$$\arccos\eta < \chi \leqslant \arccos\eta + \frac{\eta}{\sqrt{1-\eta^2}}. \tag{84}$$

As in the case of short plate solution, it is a condition put on parameter χ that is expressed in terms of both the plate length and the softening modulus K_s. It is seen that two dimensionless parameters χ and η govern the system response.

The whole interface is damaged during the subsequent delamination stage, that is for $s_1 = L$ and the value of s_2 becomes the control parameter of the loading process, so the considered situation is identical with the fourth delamination phase of the short plate solution. There are plastic and friction zones at the interface and the displacement fields are in the form of (38) and (39), with the integration constants satisfying the formulas

$$w^{p\prime}(L) = 0, \qquad w^{p}(s_2) = w^{f}(s_2) = \frac{\tau_c}{K_t} + \frac{\tau_c - \mu\sigma}{K_s}, \qquad w^{p\prime}(s_2) = w^{f\prime}(s_2).$$

They are identical with boundary and continuity conditions (57) for the fourth delamination phase of the short plate. It becomes obvious that the obtained stress and displacement fields are the same as Eqs. (58)–(63).

Fig. 10 presents a relation between the loading traction $\tau_{xy}(0)$ and the loaded end displacement $w(0)$ for various values of dimensional parameter $\chi = r_s L$ and $\zeta = K_r/K_t$. The condition (84) for a medium plate solution is satisfied. As in the previous case, the dashed line is a solution obtained for an interface with no softening effect, simply rigid–frictional interface. Similarly to the short plate solution, the delamination process cannot be realized by stress controlled loading, which would lead to dynamic response. It should be noted, that for increasing χ (plate length or the softening modulus K_s) the $\tau_{xy}(0) - w(0)$ relationship becomes steeper. The last section of the $\chi = 1.58$ curve is almost vertical which refers to the existence of only plastic and friction zones at the material interface. The scale effect is manifested by a decrease in the normalized maximum traction $\tau_{xy}(0)/\tau_{xy}^{\lim}(0)$ accompanied by an increase in plate length L, that is in the parameter χ, see Fig. 10(a). The solution in Fig. 10(b) for $\zeta = 0$ refers to a rigid–plastic–frictional interface. As in the previous case the effect of interfacial elasticity is quite strong, though the value of K_t does not enter the condition (84).

Fig. 11 presents the cohesive zone length $s_d = s_1 - s_2$ as a function of s_1, that is the length of damaged interface. The initial linear part of each plot refers to the situation when there is no frictional contact and we have only cohesive interaction. In such a case there is simply $s_d = s_1$. The subsequent nonlinear section depicts the influence of frictional stress upon the cohesive zone length. Fig. 11 presents the solution in terms of dimensionless parameter $\zeta = K_r/K_t$ and depicts the influence of interfacial elasticity. For $\zeta = 0$ we have a rigid–plastic–frictional interface, for $\zeta = 1$ the bonding is elastic-perfectly brittle. An interesting fact should be noted at this point, that is the end effect. For ζ close to zero the fully

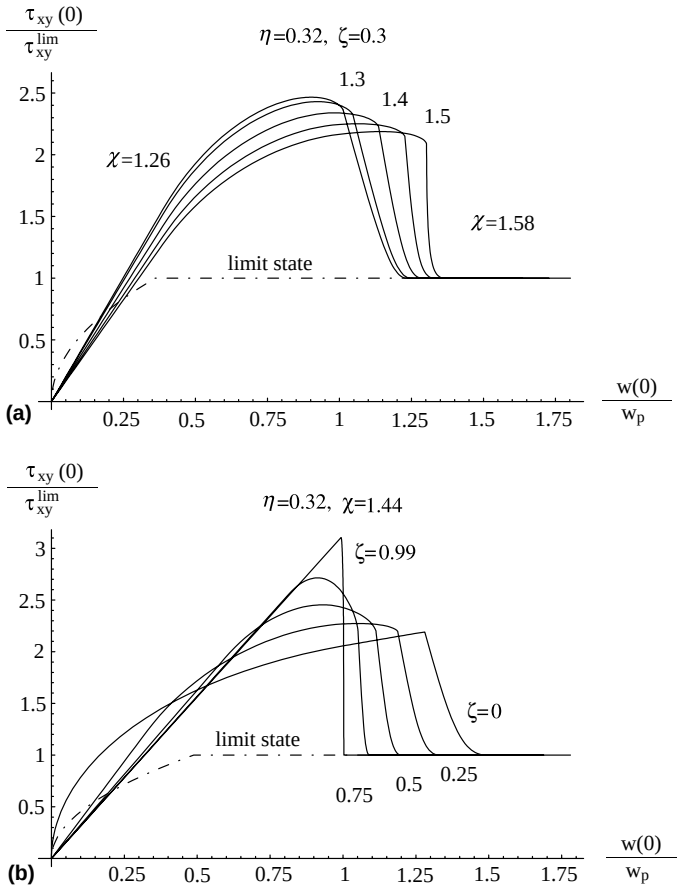

Fig. 10. Medium length solution. The loading traction $\tau_{xy}(0)$ versus loaded end displacement $w(0)$ for: (a) various values of $\chi = r_s L$—the influence of plate length L; (b) various values of $\zeta = K_r/K_t$—the influence of interface compliance with respect to its softening response; $\zeta = 0$, rigid–softening–frictional interface; $\zeta = 1$, perfectly brittle interface. The dashed line refers to the rigid–frictional model of the interface.

developed cohesive zone has a constant length for almost entire delamination process. Its value can be approximated by $\arccos \eta/r_s$ (see Mróz and Białas, accepted for publication). However, when the cohesive interface approaches the stress free end $x = L$, its length starts to increase. This is due to an interaction with the boundary $x = L$. This end effect is not present in the case of rigid–softening interface (refer to Mróz and Białas, accepted for publication), where the cohesive zone has a constant length equal exactly $\arccos \eta/r_s$. For ζ approaching unity, there is no stabilization in the length of cohesive zone for any particular loading stage. The perfectly brittle character of interfacial softening leads to instantly increasing value of s_d.

Fig. 12 presents response domains provided by conditions (51) and (82) for short, medium and long solution types in $\{\chi, \eta\}$ plane. It allows for a prediction of structure response when a set of geometry and material properties is given. It should be noted that conditions (51) and (82) do not depend on the bond elasticity coefficient K_t. Thus, presented solution types remain unchanged by the interface stiffness, though it influences the overall system response.

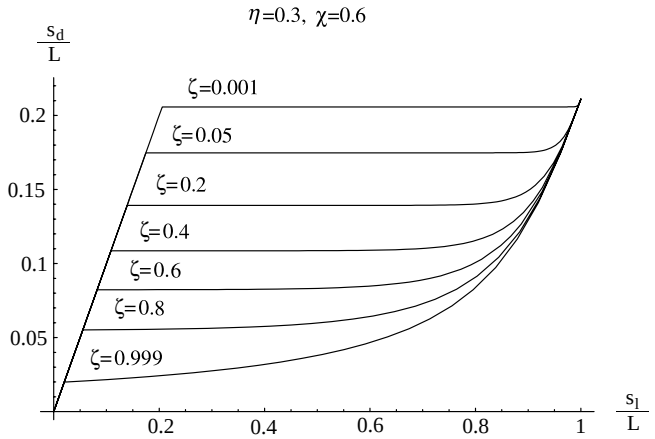

Fig. 11. The development of cohesive zone length $s_d = s_1 - s_2$ as a function of s_1. The influence of interface compliance with respect to its softening response $\zeta = K_r/K_t$; $\zeta = 0$—rigid–softening–frictional interface; $\zeta = 1$—perfectly brittle interface.

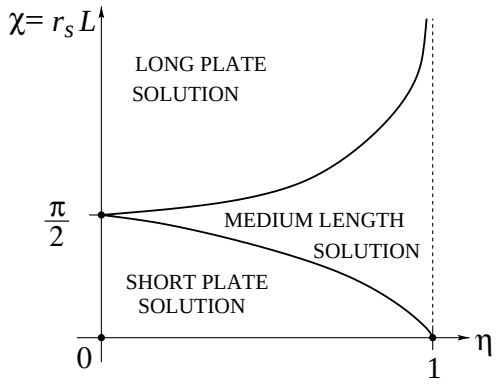

Fig. 12. Response domains in the plane $\{\chi, \eta\}$.

3.3. Long plate solution

Let us consider now a long plate solution, that is a situation when the material and geometric parameters satisfy the following condition:

$$\chi = r_s L > \arccos\eta + \frac{\eta}{\sqrt{1-\eta^2}}.$$

The first three delamination stages are the same as in the case of a medium plate, that is there are following zones at the interface:

- first phase: elastic zone,
- second phase: plastic and elastic zones,
- third phase: friction, plastic and elastic zones.

Analysis of the derivative $\partial w^{f}(x,s_1)/\partial s_1$ performed in the previous section revealed existence of a region where the plate exhibits reverse displacement. The coordinate s_3 of the transition point is provided by Eq. (81) and it monotonically increases with increasing control parameter s_1. The delamination process for this failure phase is schematically presented in Fig. 13. The length of reverse displacement zone increases and reaches its maximal value for $s_1 = L$:

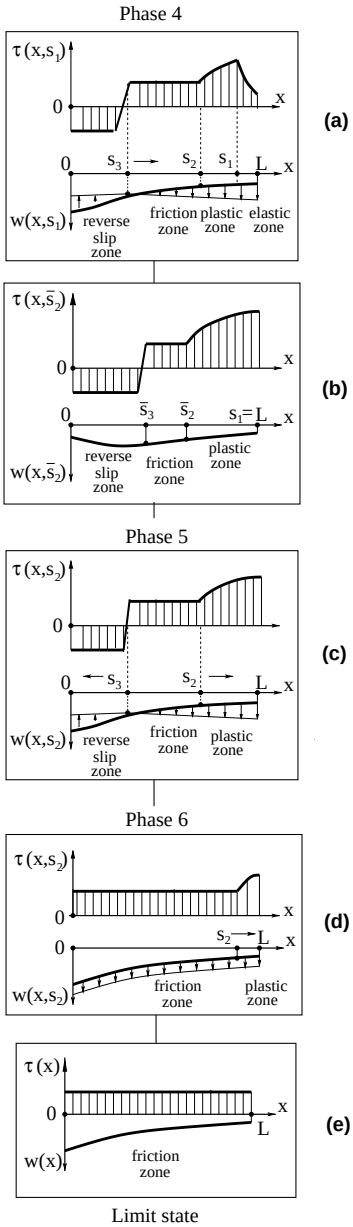

Fig. 13. Long plate solution. Delamination phases.

$$\bar{s}_3(s_1 = L) = L - \frac{1}{r_s}\arccos\eta - \frac{\eta}{r_s\sqrt{1-\eta^2}}, \tag{85}$$

that is when the elastic zone vanishes.

There are following zones developed at the interface during the subsequent loading stage: plastic, friction and reverse slip. The control parameter now is s_2—the coordinate of the transition point between plastic and friction zones. The progressive delamination of the plate is executed by a monotonic increase of s_2 from $\bar{s}_2$ to L, where

$$\bar{s}_2 = L - \frac{1}{r_s}\arccos\eta,$$

with $\bar{s}_2$ being the value of $s_2(s_1)$ for $s_1 = L$, see Eq. (67). The displacement and stress fields for the plastic and friction zones are given by:

- plastic zone, $s_2 \leqslant x \leqslant L$:

$$w^{\mathrm{p}}(x, s_2) = \frac{\tau_c}{K_t} + \frac{\tau_c}{K_s} - \frac{\mu\sigma}{K_s}\frac{\cos[r_s(L-x)]}{\cos[r_s(L-s_2)]}, \tag{86}$$

$$\tau^{\mathrm{p}}_{xy}(x, s_2) = \frac{\mu\sigma}{K_s} r_s G \frac{\sin[r_s(L-x)]}{\cos[r_s(L-s_2)]}, \tag{87}$$

$$\tau^{\mathrm{p}}(x, s_2) = \mu\sigma\frac{\cos[r_s(L-x)]}{\cos[r_s(L-s_2)]}; \tag{88}$$

- friction zone, $s_3 \leqslant x \leqslant s_2$:

$$w^{\mathrm{f}}(x, s_2) = \frac{\mu\sigma}{2Gt}(x-s_2)^2 + \frac{\mu\sigma r_s}{K_s}\tan[r_s(L-s_2)](x-s_2) + \frac{\tau_c - \mu\sigma}{K_s} + \frac{\tau_c}{K_t}, \tag{89}$$

$$\tau^{\mathrm{f}}_{xy}(x, s_2) = -\frac{\mu\sigma}{t}(x-s_2) - \frac{\mu\sigma r_s G}{K_s}\tan[r_s(L-s_2)], \tag{90}$$

$$\tau^{\mathrm{f}}(x, s_2) = \mu\sigma. \tag{91}$$

Let us note that Eqs. (86)–(91) are identical to (58)–(63) since they refer to the same displacement fields as well as the boundary and continuity conditions. However, the fields (89)–(91) cannot be accepted as the correct solution since the rate of deflection changes its sign within the frictional interface. In fact, the derivative:

$$\frac{\partial w^{\mathrm{f}}(x, s_2)}{\partial s_2} = 0 \tag{92}$$

vanishes at $x = s_3$ and becomes negative for $0 \leqslant x \leqslant s_3$. Thus, there is a transition point between the forward ($\dot{w}^{\mathrm{f}} > 0$) and the reverse ($\dot{w}^{\mathrm{f}} < 0$) displacement zones. By substituting (86) into Eq. (92), one obtains a formula relating s_3 to the loading parameter s_2:

$$s_3 = s_2 - \frac{1}{r_s}\cot[r_s(L-s_2)]. \tag{93}$$

The value of s_3 decreases from $\bar{s}_3$ to minus infinity when s_2 increases from $\bar{s}_2$ and approaches L, meaning that the length of reverse displacement zone becomes shorter. It has been schematically presented in Fig. 13.

After the reverse displacement zone has vanished, there are two regions at the interface: plastic and friction. The displacement and stress fields are respectively provided by Eqs. (58)–(63). This delamination phase is associated with the progressive slip and the evolution of s_2 to its limit value L, when the plastic zone is erased and the limit state is reached.

We shall analyze now the displacement and stress fields at the reverse slip zone. Detailed analytical solution requires two more interfacial regions to be considered, namely elastic unloading and frictional unloading with the shear stress τ equal $-\mu\sigma$. However, this would further complicate the equations, since the loading history should then be included in the analysis. A numerical solution will be constructed for the reverse displacement region $0 \leqslant x \leqslant s_3$. Eqs. (86)–(91) derived for the remaining section of the plate $s_3 \leqslant x \leqslant L$ still hold.

Let us divide the region $0 \leqslant x \leqslant \bar{s}_3$ into finite differences of length Δx, where the value $\bar{s}_3$ is given by (85). Thus, we have chosen n points lying in the interval $0 \leqslant x \leqslant \bar{s}_3$ as indicated in Fig. 14. As discussed previously, during the fourth loading phase the length s_3 of reverse displacement zone increases from zero to $\bar{s}_3$ and then subsequently decreases to zero. It should be noted, that we have provided analytical expressions for displacement fields $w(x)$, where x belongs to the interval $s_3 \leqslant x \leqslant L$. Therefore, the values $w(s_3)$, $w'(s_3)$, $w''(s_3)$ are also known.

Let us assume that during the forth loading phase, that is when the reverse displacement zone develops at the interface, its length s_3 subsequently takes the following values:

$$x_1 = 0, \quad x_2 = \Delta x, \quad x_3 = 2\Delta x, \quad \ldots, \quad x_n = \bar{s}_3.$$

Let us denote by $w_{i,j}$ the plate displacement at point x_i when s_3 is equal to x_j. By making use of Taylor series expansion we can write:

$$w_{i,j} = w_{i+1,j} - w'_{i+1,j}\Delta x + \tfrac{1}{2} w''_{i+1,j}\Delta x^2, \tag{94}$$

where $w'_{i+1,j}$, $w'_{i+1,j}$ are first and second derivatives of w function at point x_{i+1} for s_3 equal to x_j. Since the values $w(s_3)$, $w'(s_3)$, $w''(s_3)$ are known, the formula (94) provides the displacement $w_{j-1,j}$.

Let us define the trial interfacial stress at point x_i:

$$\tau_i^{\text{trial}} = K_t(w_{i,j} - w_{i,j-1}) + \tau_{i,j-1}. \tag{95}$$

Thus, the τ_i^{trial} stress refers to elastic unloading of the interface. If the following condition is satisfied:

$$|\tau_i^{\text{trial}}| \leqslant \mu\sigma, \tag{96}$$

we have an elastic unloading only and

$$\tau_{i,j} = \tau_i^{\text{trial}}.$$

If the condition (96) is not satisfied, then there is a frictional stress at the interface and we have:

$$\tau_{i,j} = \mu\sigma \operatorname{sign}(w_{i,j} - w_{i,j-1}). \tag{97}$$

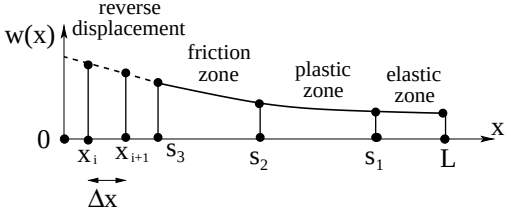

Fig. 14. Division of the reverse displacement zone into finite differences of length Δx.

When the value of $\tau_{i,j}$ is known, the second derivative of function $w(x)$ at point x_i is provided by

$$w''_{i,j} = \frac{\tau_{i,j}}{Gt}, \tag{98}$$

being analogous to expression (33).

The $w'_{i,j}$ derivative can be obtained from the Taylor series expansion. From formula

$$w_{i+1,j} = w_{i,j} + w'_{i,j}\Delta x + \tfrac{1}{2}w''_{i,j}\Delta x^2,$$

one can derive $w'_{i,j}$ in the form:

$$w'_{i,j} = \frac{w_{i+1,j} - w_{i,j}}{\Delta x} - \frac{1}{2}w''_{i,j}\Delta x. \tag{99}$$

The expressions (94), (98), and (99) provide the displacement w and the derivatives w', w'' at point x_i. Subsequently, we move to x_{i-1} point and derive these quantities by using the same algorithm. Thus, for a given length s_3 we know the displacement and stress state at every point x_i, $i = 1,\ldots,n$ within the reverse displacement zone.

After the elastic interfacial zone has disappeared, the loading parameter is s_2. We continue to use the same algorithm for displacement and stress fields within the reverse displacement zone. On contrary to the previous delamination phase, the length s_3 of reverse displacement zone decreases now from $\bar{s}_3$ to zero and the values of w, w' and w'' at point s_3 are derived from Eq. (89).

When the reverse displacement zone has vanished, there are plastic and friction zones left at the interface. The displacement and stress fields are provided by Eqs. (58)–(63). The interface is fully damaged when the value of s_2 reaches L.

After the reverse displacement zone has vanished, there are two regions at the interface: plastic and friction. The displacement and stress fields are respectively specified by formulas (58)–(63). This delamination phase is associated with the progressive slip and the evolution of s_2 to its limit value L. Then, the plastic zone is erased and the limit state is reached as discussed previously.

The present solution describes the quasi-static response assuming the process to be controlled by the progressive front of the plastic zone. Fig. 15 reveals a complex system response. It is seen that in order to perform the progressive delamination, a cyclic loading along a specific loading path is required. The number of hysteretic loops in the $\tau_{xy}(0) - w(0)$ relation depends on the value of dimensionless parameter χ. By keeping the K_s constant and varying only the plate length L, we obtain a different number of loops. The number of loading cycles required to damage the interface increases with increasing L. The results show that the part of the structure in the $x \in \langle 0, \bar{s}_3 \rangle$ zone performs a flattering movement with subsequent forward and reverse displacements. This process cannot be executed either by stress or displacement controlled loading. In practice it may lead to an unstable behaviour with a critical point related to the disappearance of undamaged interfacial area. A dynamic mode could follow next starting from this limit state. However, the present solution clarifies the nature of critical points associated with the delamination process and can provide a reference solution for numerical algorithms attempting to generate equilibrium paths in the post-critical states. The reason for the combined decrease in loading traction and loaded end displacement is the elastic energy, stored in the plate during the previous loading phase and being released to debond the structure. For a longer plate there is more elastic energy in the structure and consequently a greater number of loading cycles is required for its dissipation at the frictional interface. Any extra work by external forces would result in a dynamic response.

Fig. 16 presents the effect of interfacial stiffness. The dimensional parameter ζ is defined by $\zeta = K_r/K_t$, where K_r is the interfacial softening modulus associated with irreversible slip component and K_t is the interfacial stiffness. For $\zeta = 1$ we have a brittle interface, for $\zeta = 0$ the interface is rigid–plastic. It is seen, that the value of ζ also influences the number of hysteretic cycles required to fully debond the structure. For

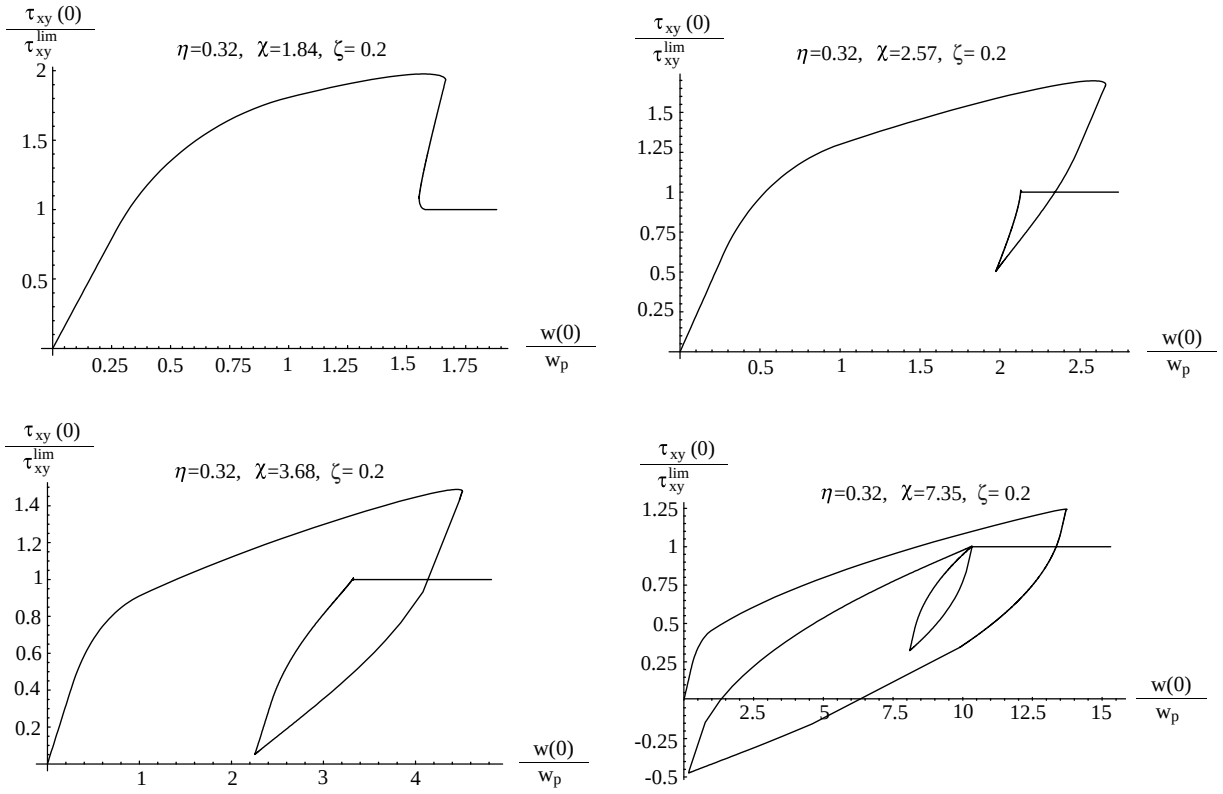

Fig. 15. Long plate solution. The loading traction versus loaded end displacement. The solutions for various values of parameter $\chi = r_s L$.

decreasing ζ the number of hysteretic loops in $\tau_{xy} \sim w(0)$ relation increases. In the limit case of $\zeta = 0$, that is for rigid–plastic interface, the number of loading cycles approaches infinity. It is important to notice, that the interfacial elasticity is required to construct the complete quasi-static solution. In the companion paper Mróz and Białas (accepted for publication), a rigid–softening interfacial model was considered. Due to the discontinuity in the constitutive relation for the interface, it was impossible to construct a complete solution for a long plate case. The present approach explains this phenomena stating that for an increasing stiffness an increasing number of hysteretic loops is required, approaching infinity in the limit case.

In the paper by Schreyer and Peffer (2000), a fiber pullout problem was treated by reflecting the effect of deformable medium surrounding a fiber by an interface, with the surrounding medium assumed to be rigid. The fiber was treated as an elastic body and three-dimensional effects associated with normal stresses due to Poisson's ratio were neglected. In the case of progressive interfacial failure, the shear stress at the interface was assumed to be a linearly increasing function of relative tangential displacement. When a critical state was reached, the stress decreased linearly to zero, resulting in no traction at contact for a fully damaged interface. The present model provides results obtained by Schreyer and Peffer (2000) by setting $\mu\sigma = 0$, that is for the frictionless case. It should be noted that in the case of frictionless solution, the progressive delamination does not lead to a hysteretic response in the loading stress–loaded end displacement relation. The loading force either decreases to zero with increasing displacement, or there is a combined decrease of loading force and loaded end displacement leading to interfacial failure (see Schreyer and Peffer, 2000).

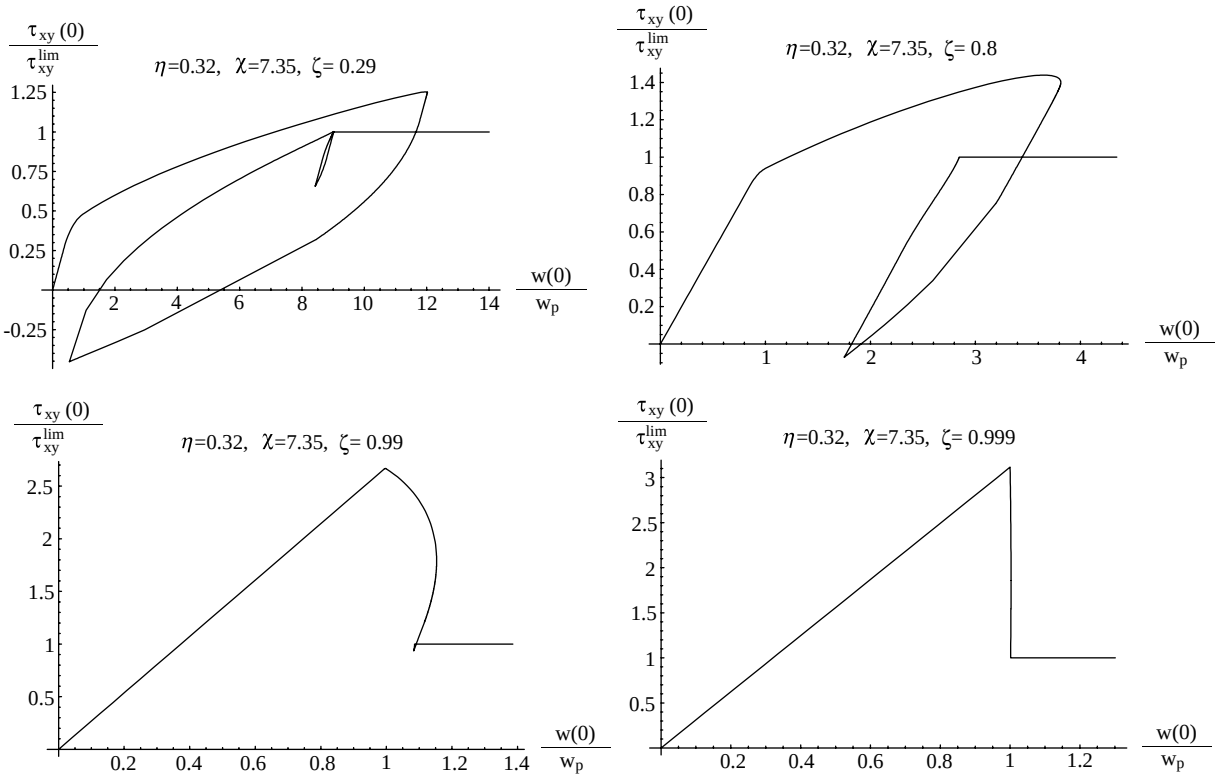

Fig. 16. Long plate solution. The loading traction versus loaded end displacement. The solutions for various values of parameter $\zeta = K_r/K_t$; $\zeta = 1$—brittle interface; $\zeta = 0$—rigid–plastic interface.

4. Finite element validation

In the present section we shall compare the obtained analytical results of the shear beam model with a finite element analysis of an elastic plate bonded to a rigid substrate by a cohesive interface. The problem presented in Fig. 5 shall be treated as two dimensional, with elastic plane stress elements for the plate material and with zero thickness interfacial elements.

As a starting point for the derivation of the finite element equations, we take the week form of equilibrium equation (4):

$$\int_{\Omega} \boldsymbol{\sigma} : \nabla \delta \boldsymbol{w} \, \mathrm{d}\Omega + \int_{S_{\mathrm{inter}}} (T_{\mathrm{n}} \delta d_{\mathrm{n}} + T_{\mathrm{t}} \delta d_{\mathrm{t}}) \, \mathrm{d}S = \int_{S_{\mathrm{ext}}} \boldsymbol{t} \delta \boldsymbol{w} \, \mathrm{d}S, \tag{100}$$

where $\delta \boldsymbol{w}$ stands for kinematically admissible virtual displacement and δd_{n} and δd_{t} are the virtual relative displacements at the interface, respectively for normal and tangential separation. The integral over S_{inter} is the work of interface normal and shear stresses on the displacement discontinuity, whereas the remaining formulas in Eq. (100) resemble the standard weak formulation of equilibrium equation.

The vector $\{d_{\mathrm{n}}, d_{\mathrm{t}}\}^{\mathrm{T}}$ of relative displacements along the interface reduces in our case to the plate displacement field $\boldsymbol{w}$, since the structure is bonded to a rigid substrate. An interface element is presented in Fig. 17, with nodes 5, 6, 7, 8 assumed to have zero displacements, as they are a part of the rigid substrate surface. Let us denote the displacements of node α ($\alpha = 1, 2, 3, 4$) by w_{β}^{α} and w_{ξ}^{α} for tangential displacements

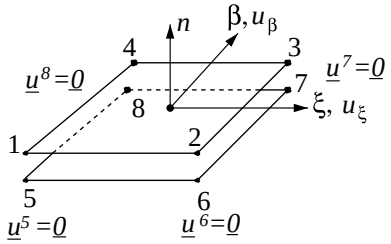

Fig. 17. Finite element of the interface.

respectively along β and ξ axes. Assuming the linear approximation of the relative displacement field along the interface element, we have:

$$w_\xi(\xi,\beta) = N_1 w_\xi^1 + N_2 w_\xi^2 + N_3 w_\xi^3 + N_4 w_\xi^4,$$
$$w_\beta(\xi,\beta) = N_1 w_\beta^1 + N_2 w_\beta^2 + N_3 w_\beta^3 + N_4 w_\beta^4,$$

where the shape functions N_i are of the form:

$$N_i = \tfrac{1}{4}(1+\xi_i\xi)(1+\beta_i\beta).$$

In order to describe the delamination process, we shall use the incremental constitutive relations formulated in Section 2.1. The interface is subjected to compressive stresses and the yield function F is given by Eq. (16), whereas the non-associated plastic potential by Eq. (18).

Time discretization provides the following set of equations:

$$\boldsymbol{w}_{n+1}^{\mathrm{e}} = \boldsymbol{w}_{n+1} - \boldsymbol{w}_{n+1}^{\mathrm{s}}, \tag{101}$$

$$\boldsymbol{\tau}_{n+1} = K_{\mathrm{t}} \boldsymbol{w}_{n+1}^{\mathrm{e}}, \tag{102}$$

$$\boldsymbol{w}_{n+1}^{\mathrm{s}} = \boldsymbol{w}_{\mathrm{n}}^{\mathrm{s}} + \Delta\lambda_{n+1} \frac{\partial \Phi(\boldsymbol{\tau}_{n+1})}{\partial \boldsymbol{\tau}}, \tag{103}$$

$$\psi_{n+1} = \psi_n + \frac{K_{\mathrm{r}}}{\tau_{\mathrm{c}}^0} \Delta\lambda_{n+1}, \tag{104}$$

$$F = |\boldsymbol{\tau}| + \mu\sigma - \tau_{c_{n+1}} = 0, \tag{105}$$

$$\Phi = |\boldsymbol{\tau}|, \tag{106}$$

where the parameter ψ describes the softening process, $(\cdot)_n$ stands for the previous state and $(\cdot)_{n+1}$ refers to the current, or unknown, state. The value of K_{r} is the softening modulus associated with the plastic slip component. The relation between K_{r} and K_{s} is given by Eq. (25).

Assuming the linear degradation of critical shear stress τ_{c} as a function of inelastic displacement w^{s} we have:

$$\tau_{c_{n+1}} = \begin{cases} \tau_{\mathrm{c}}^0(1-\psi_{n+1}), & \psi_{n+1} \leqslant 1, \\ 0, & \psi_{n+1} > 1. \end{cases} \tag{107}$$

For $\psi > 1$ the interface is fully damaged and there is only frictional interaction at the interface.

By making use of the fully implicit integration scheme, we seek for a solution satisfying the yield function (105) and the flow rule (103) at the end of each time step. Since the process is displacement controlled, for a

given displacement increment $\Delta \boldsymbol{w}_{n+1} = \boldsymbol{w}_{n+1} - \boldsymbol{w}_n$ we postulate a trial shear stress at the interface in the form:

$$\boldsymbol{\tau}_{n+1}^{\text{trial}} = \boldsymbol{\tau}_n + K_{\text{t}} \Delta \boldsymbol{w}_{n+1}. \tag{108}$$

If for the stress $\boldsymbol{\tau}_{n+1}^{\text{trial}}$ we have $F < 0$, then there is no failure evolution associated with the displacement increment $\Delta \boldsymbol{w}_{\text{n+1}}$ and the shear stress $\boldsymbol{\tau}$ equals $\boldsymbol{\tau}_{n+1}^{\text{trial}}$. For $\boldsymbol{\tau}_{n+1}^{\text{trial}}$ yielding $F > 0$ we have an interfacial failure development and the amount of irreversible slip $\boldsymbol{w}_{n+1}^{\text{s}}$ and current values of parameters ψ_{n+1} and $\Delta\lambda_{n+1}$ are obtained simultaneously from Eqs. (103)–(105) by using the Newton–Raphson iteration scheme. The elastic slip and the shear stress at the interface are then calculated respectively from Eqs. (101) and (102).

The plate material is modeled by two dimensional plane stress elements. Thus, the value of uniform normal traction σ acting on the upper plate surface does produce neither any stresses nor structural displacements and only enters the yield function (105) as a loading parameter.

Let us assume that the plate is a granite block with the value of Young modulus equal to $E = 4 \times 10^4$ MPa and Poisson's ratio $v = 0.25$. The shear strength is $\tau_{\text{c}}^0 = 30$ MPa and the friction coefficient $\mu = 0.64$. The resulting Kirchhoff modulus is $G = 1.6 \times 10^4$ MPa. The plate dimensions are $L = 2$ m, $b = 4$ m, $t = 0.2$ m in order to provide the anti-plane shear state. The traction σ acting on the upper surface has the value $\sigma = 20.1$ MPa and the resulting friction stress for the fully damaged interface is $\mu\sigma = 12.9$ MPa. The value of the dimensionless parameter $\eta = \mu\sigma/(\mu\sigma + \tau_{\text{c}}^0)$ equals $\eta = 0.3$. By varying the interfacial softening modulus K_{s}, we can obtain the delamination scenario characteristic for short, medium and long plate solutions.

According to the analytical results for the shear beam model, in order to obtain a short plate solution, the dimensionless parameter χ has to satisfy the inequality:

$$\chi = \sqrt{\frac{K_{\text{s}}}{Gt}} \leqslant \arccos \eta = \arccos 0.3 = 1.2661.$$

For the subsequent simulation of short plate delamination the value of $K_{\text{s}} = 800$ MPa/m has been assumed which, with the values of G and t already introduced, satisfies the short plate condition.

The delamination process is displacement controlled by an increasing value of displacement $u_y(y, x = 0)$ of plate boundary for $x = 0$. It has been assumed that the displacement $u_x(y, x = 0)$ in x direction is constrained, that is we have $u_x(y, x = 0) = 0$.

Fig. 18 presents the relation between the displacement u_x and the stress τ_{xy} at point 0, that is at the origin of coordinate system, see Fig. 5. The continuous line was obtained using the analytical solution for the

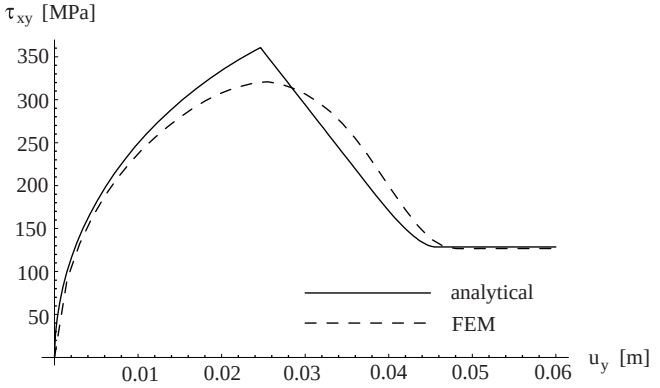

Fig. 18. Load–displacement curves for the short plate solution: dashed line—results of numerical simulation for two dimensional model; continuous line—analytical solution for shear-beam model.

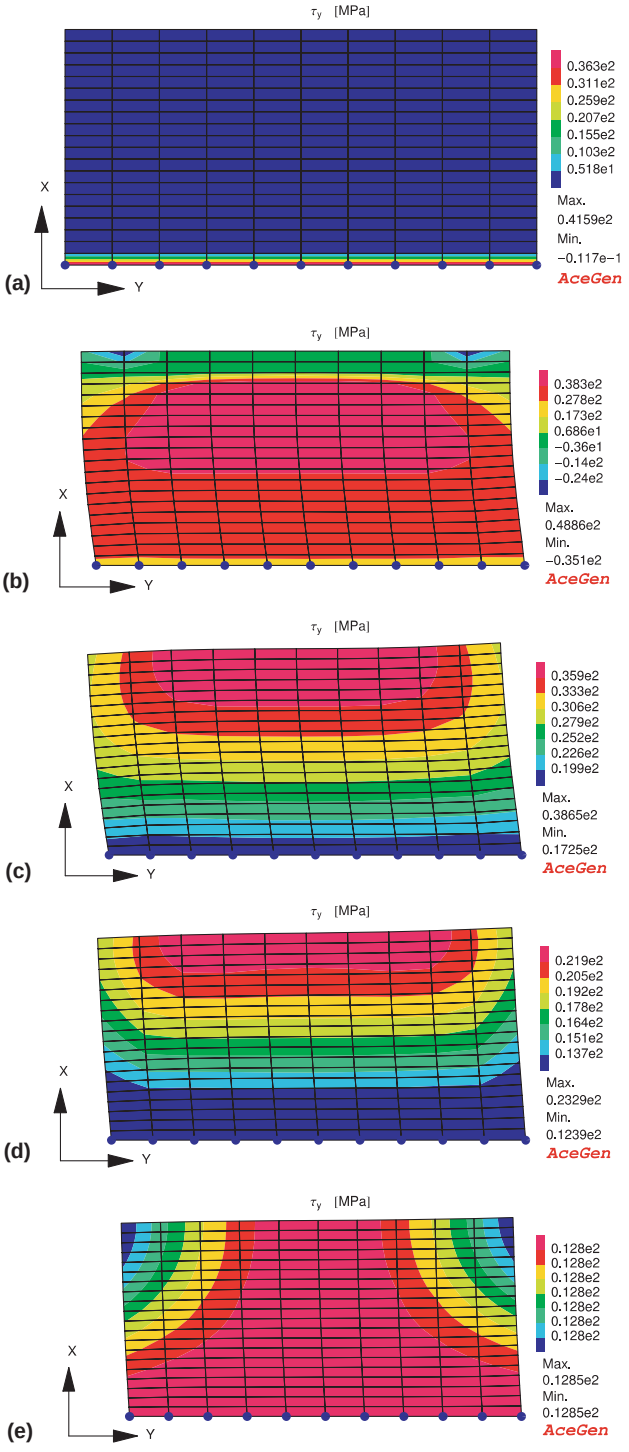

Fig. 19. The variation of interfacial shear stress τ_y [MPa] during the course of delamination for the short plate response; the subsequent displacements u_y of boundary $x = 0$: (a) 26×10^{-6} m, (b) 0.02 m, (c) 0.032 m, (d) 0.042 m, (e) 0.06 m.

shear beam model, whereas the dashed line is a result of numerical simulation performed for the two dimensional system. The simulation results are very close to the analytical solution during the early delamination stages. As the failure progresses though, the differences become more visible and disappear only during the last delamination stage, that is when there is only frictional interaction at contact. It is seen, that the decrease of loading force is smoother in the case of two dimensional simulation.

Fig. 19(a)–(e) present the variation of interfacial shear stress τ_y during the delamination process obtained for the following values of displacement at point 0: 26×10^{-6} m, 0.02 m, 0.032 m, 0.042 m, 0.06 m. For clarity, the deformed mesh has been magnified and does not present the exact solution for the displacement field. Fig. 19 were obtained for subsequent delamination phases of short plate and thus we have: in (a) the interface is fully elastic and the shear stress is below the critical value τ_c; in Fig. 19(b) the interface is in the elastic and plastic regimes; Fig. 19(c) presents the evolution of interfacial plastic zone; Fig. 19(d) shows both plastic and frictional stresses at the interface, whereas in Fig. 19(e) only frictional stress for fully damaged interface is presented. The τ_y stress presents a slight dependence on the y coordinate, so interfacial zones of elastic, plastic and frictional stresses are not exactly parallel. This is due to the flexural effects still present during the course of delamination and playing a dominant role mainly along the stress free boundaries. Moreover, as presented in Fig. 19(e), the fully frictional interface becomes unloaded below the frictional stress value $\mu\sigma = 12.9$ MPa, which is also a result of flexural response of the structure.

Let us discuss now the medium length plate delamination. The dimensionless parameter χ has to satisfy the condition:

$$\arccos\eta < \chi \leqslant \arccos\eta + \frac{\eta}{\sqrt{1-\eta^2}}.$$

For the simulation the softening modulus K_s equal to $K_s = 1800$ MPa/m, satisfying the above inequality, has been assumed.

Fig. 20 presents the relation between the displacement u_x and the stress τ_{xy} at point 0, that is at the origin of coordinate system. The continuous line was obtained using the analytical solution for the shear beam model, whereas the dashed line is a result of numerical simulation performed for the two dimensional system. As in the case of short plate solution, the simulation is very close to the analytical solution during the early delamination stages. As the failure progresses though, the differences become more visible. In particular, the delamination stage associated with the decrease in loading force after the elastic zone has been terminated, is significantly different. The shear beam model provides an abrupt jump in the value of loading traction, whereas the numerical simulation results in a more compliant system response. The differences

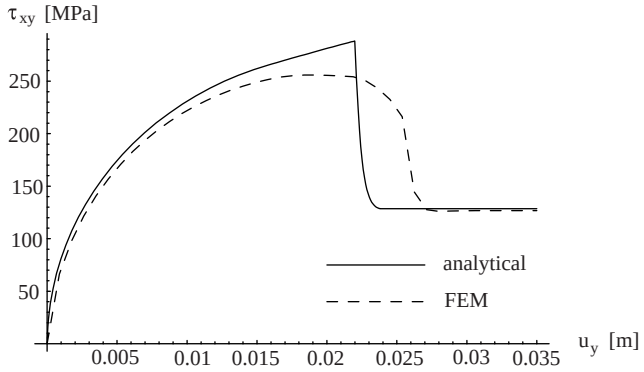

Fig. 20. Load–displacement curves for the medium plate solution: dashed line—results of numerical simulation for two dimensional model; continuous line—analytical solution for shear-beam model.

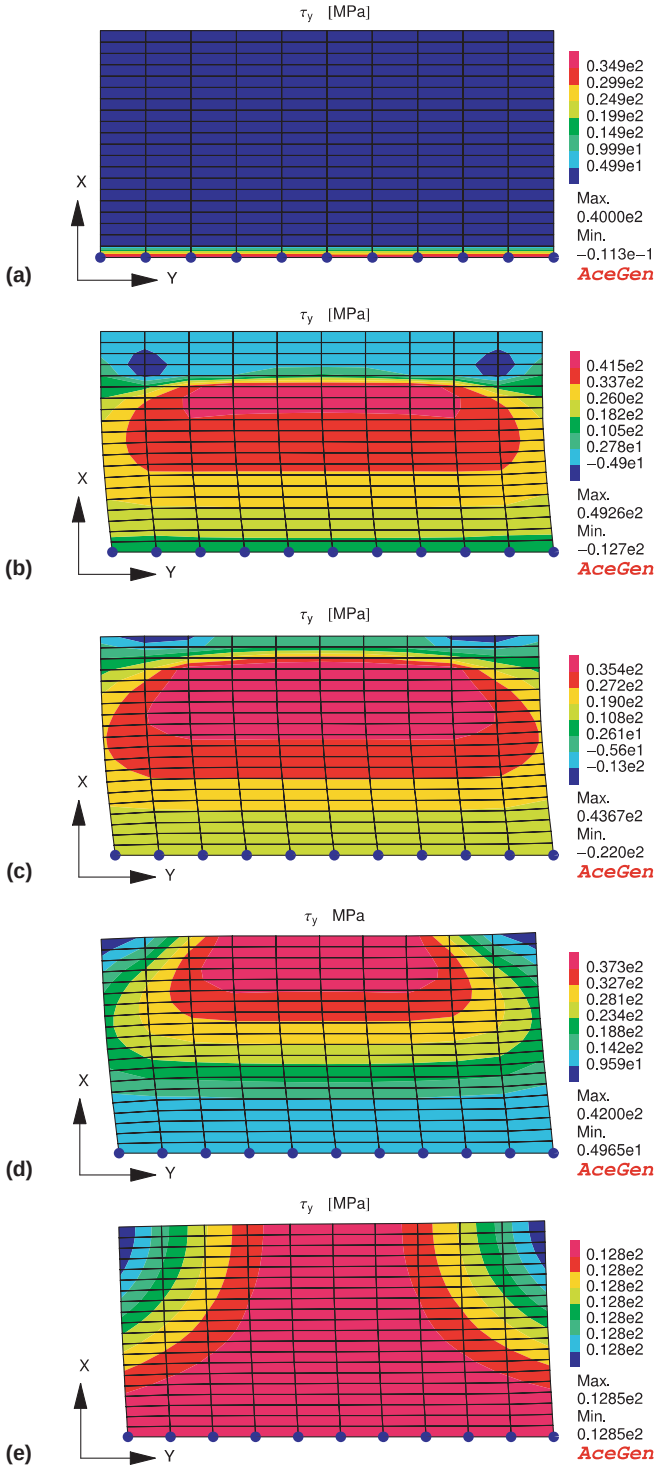

Fig. 21. The variation of interfacial shear stress τ_y [MPa] during the course of delamination for the medium length response; the subsequent displacements u_y of boundary $x = 0$: (a) 25×10^{-6} m, (b) 0.015 m, (c) 0.019 m, (d) 0.023 m, (e) 0.035 m.

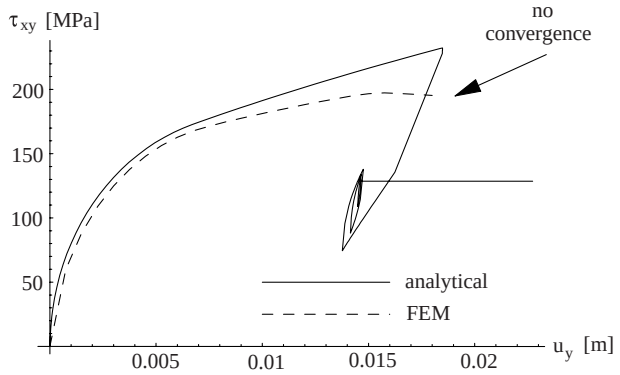

Fig. 22. Load–displacement curves for the long plate solution: dashed line—results of numerical simulation for two dimensional model; continuous line—analytical solution for shear-beam model.

between the finite element simulation and the analytical model are more visible than in the case of short plate solution.

Fig. 21(a)–(e) present the variation of interfacial shear stress τ_y during the delamination process, obtained for the following displacement values at point 0: 25×10^{-6} m, 0.015 m, 0.019 m, 0.023 m, 0.035 m. As in the previous case, the deformed mesh has been magnified and does not present the exact solution for the displacement field. Fig. 21 were obtained for subsequent delamination phases for the medium plate and thus we have: in (a) the interface is fully elastic and the shear stress is below the critical value τ_c; in Figure (b) the interface is in both elastic and plastic regimes; Figure (c) presents the evolution of frictional, plastic and elastic zones; Figure (d) shows both plastic and frictional stresses at the interface, whereas in Figure (e) only frictional stress for fully damaged interface is presented. The τ_y stress presents a slight dependence on the y coordinate since the interfacial zones of elastic, plastic and frictional stresses are not exactly parallel. As in the case of short plate solution, this is due to the flexural effects still present during the course of delamination and playing a dominant role mainly along the stress free boundaries. Again, as presented in Fig. 21(e), the fully frictional interface becomes unloaded below the frictional stress value $\mu\sigma = 12.9$ MPa, which is also a result of flexural response of the structure. Let us note that flexural interaction with frictional foundation leads to the effect of slip patterning with an infinite set of progressive an reversive slip zones at the contact, cf. Stupkiewicz and Mróz (1994).

For $K_s > 1999$ MPa/m we have a long plate solution. Due to the numerical convergence problems, the full delamination process could not be performed. These difficulties arise from the fact, that displacement controlled simulation does not lead to a progressive failure evolution and the quasi-static equilibrium path cannot be generated. Fig. 22 presents the solution for $K_s = 4500$ MPa/m obtained only up to the point of loss of convergence. It is associated with the first loop in the load-displacement curve for the shear beam model. Thus, the simple model of decohesion provides a reference solution for numerical algorithms searching for quasi-static equilibrium paths in more complex cases.

5. Summary and conclusions

The present work aimed at analytical and numerical solutions of anti-plane shear damage growth at an interface between a plate and a rigid foundation. The concept of cohesive zone ahead of crack tip was used in order to simulate progressive damage and ultimate failure. A particular attention was given to the analysis of critical and post-critical states associated with growth of delamination zone under monotonic

loading. The analytical quasi-static solution was obtained by neglecting plate flexural effects and assuming linear softening constitutive relation for the interface. The control parameter driving the failure process was the length of damage zone. The analytical results were next validated by a finite element analysis of plate delamination under plane stress conditions, bonded to a rigid substrate. It was shown that the types of response can be specified in terms of two dimensionless parameters χ and η, with corresponding short, medium and long plate solutions. Subsequently, there are following zones developed at the interface for the short plate solution:

1. elastic,
2. cohesive and elastic,
3. cohesive,
4. friction and cohesive,
5. friction.

The medium plate solution is characterized by the subsequent delamination phases:

1. elastic,
2. cohesive and elastic interfacial zones,
3. friction, cohesive and elastic zones,
4. friction and cohesive zones,
5. friction zone.

The long plate solution, being the most complex one, is characterized by the following scenario:

1. elastic,
2. cohesive and elastic interfacial zones,
3. friction, cohesive and elastic zones,
4. reverse displacement, friction, cohesive and elastic zones,
5. reverse–forward displacement, friction and cohesive zones,
6. friction and cohesive zones,
7. friction zone.

In the case of both short and medium plate solutions, the unstable system response was related to a sudden decrease in the loading traction. It was associated with the end effect, that is the interaction between the interfacial cohesive zone and the stress free end at $x = L$. Thus, the delamination process cannot be executed by stress controlled loading, since it would lead to a dynamic behaviour. A displacement controlled loading should be used, since it leads to a stable response, resulting in a fully damaged interface with frictional interface tractions in the limit state. It was shown that the interfacial compliance defined by dimensionless parameter ζ can significantly change the structural response, though it does not influence the overall conditions defining short, medium and long plate solution types.

For the long plate solution there appear reverse slip zones with snap back response of the loaded boundary. In order to execute a quasi-static delamination both the loading traction and the loading end displacement should follow a unique equilibrium path, resulting in a hysteretic response. The structure close to the loaded end performs a flattering movement with subsequent forward and reverse displacements. The number of cycles leading to complete delamination is dependent on dimensionless parameter χ, that is on the plate length. The reason for the combined traction and displacement interaction is the elastic energy stored in the plate and next released to debond the structure. Thus, an extra work by external forces would be transformed into kinetic energy and a dynamic mode would follow. It was shown, that the number of

hysteretic cycles is also dependent on the interface stiffness captured by dimensionless parameter ζ. For a brittle interface no cycles are required to debond the structure. For increasing interfacial stiffness we have an increasing number of hysteretic loops, approaching infinity in the limit case of rigid–plastic bond.

The shear beam model was validated by a finite element analysis. It was shown, that one can neglect the flexural deformation provided that the plate width is greater than its length. The analytical solution describes qualitatively the delamination process and is close to the numerical results during the early delamination phases. Following the critical point associated with maximum value of traction subjected to the structure, differences increase and disappear only when the structure is fully debonded with frictional contact at the interface.

Displacement control does not provide a complete solution for the long plate case. There is a divergence in numerical procedure at the beginning of first hysteretic loop. Thus, the analytical shear beam model provides a reference solution for numerical algorithms searching for quasi-static equilibrium paths. A dynamic analysis would provide more clear insight into failure evolution in the final stage of damage.

Acknowledgement

The financial support of the Polish National Committee of Sciences (KBN Project No. T07A 022 20) is gratefully acknowledged.

References

Bennison, S.J., Lawn, B.R., 1989. Role of interfacial crack bridging sliding friction in the crack resistance and strength properties of non-transforming ceramics. Acta Metallurgica 37 (10), 2659–2671.

Evans, A.G., Hutchinson, J.W., 1989. Effect of non-planarity on the mixed mode fracture resistance. Acta Metallurgica 37 (3), 909–916.

Gross, T.S., Mendelsohn, D.A., 1989. Mode I stress intensity factors induced by fracture surface roughness under pure mode III loading: application to the effect of loading models on stress corrosion crack growth. Metallurgical and Materials Transactions A 20 (10), 1989–1997.

Hillerborg, A., Modeer, M., Peterson, P.E., 1976. Analysis of crack formation and crack growth in concrete by means of fracture mechanics and finite elements. Cement and Concrete Research 6, 773–782.

Hutchinson, J.W., Suo, Z., 1991. Mixed mode cracking of layered materials. In: Hutchinson, J.W., Wu, T.Y. (Eds.), Advances in Applied Mechanics, vol. 29. Academic Press, pp. 63–191.

Mróz, Z., Białas, M., accepted for publication. A simplified analysis of interface failure under compressive normal stress and monotonic or cyclic shear loading. International Journal of Numerical and Analytical Methods in Geomechanics.

Mróz, Z., Seweryn, A., 1998. Non-local failure and damage evolution rule: application to a dilatant crack model. Journal de Physique IV Pr 8 (8), 257–268.

Mróz, Z., Shen, X., 1999. Analysis of progressive interface failure under monotonic loading. In: Xu, B., Tokuda, M., Wang, X. (Eds.), Microstructures and Mechanical Properties of New Engineering Materials. International Academic Publishers, Beijing, pp. 109–114.

Mróz, Z., Stupkiewicz, S., 1995. Hysteretic effects and progressive delamination at composite interfaces. In: Pyrz, R. (Ed.), IUTAM Symposium on Microstructure—Property Interactions in Composite Materials. Kluwer Academic Publishers, pp. 247–264.

Ortiz, M., 1996. Computational micromechanics. Computational Mechanics 18 (5), 321–338.

Schreyer, H.L., Peffer, A., 2000. Fiber pullout based on a one-dimensional model of decohesion. Mechanics of Materials 32, 821–836.

Shen, X., Mróz, Z., 2000. Analysis of progressive interface failure under cyclic shear loading. Advances in Structural Engineering 3 (4), 279–290.

Stupkiewicz, S., Mróz, Z., 1994. Elastic beam on a rigid frictional foundation under monotonic and cyclic loading. International Journal of Solids and Structures 31 (24), 3419–3442.

Yang, B., Ravi-Chandar, K., 1997. Antiplane shear crack growth under quasistatic loading in damaging material. International Journal of Solids and Structures 35 (28–29), 3695–3715.